



Planetary and Solar Radio Occultation/Scintillations:

With an Emphasis on Interplanetary Scintillation (IPS) and Heliospheric Faraday Rotation (FR).

*Dr. Mario M. Bisi (Institute of Mathematics and
Physics, Aberystwyth University, Wales, UK) –*

Mario.Bisi@aber.ac.uk

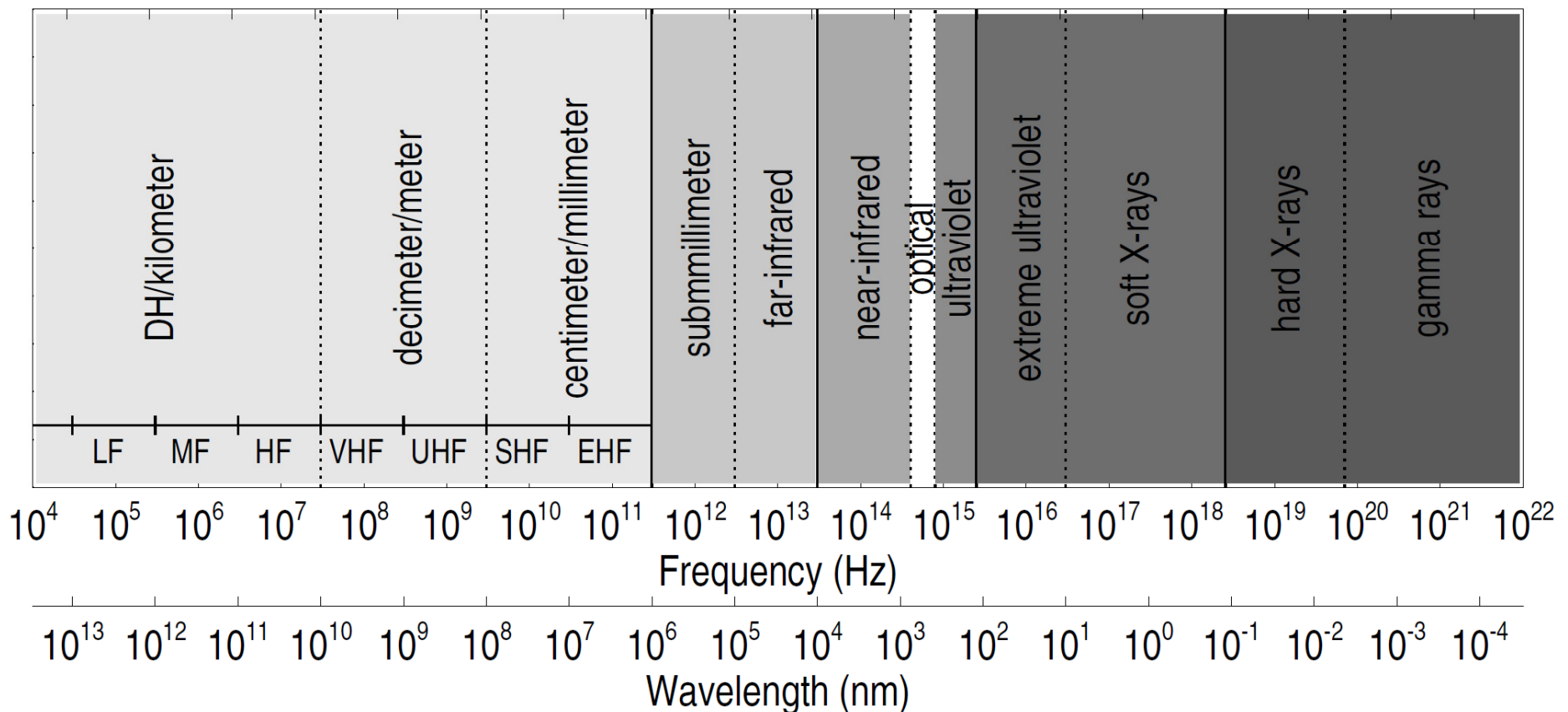
Lecture Outline

- ❖ A Brief Introduction to the Radio Spectrum!
 - ❖ What is Occultation?
 - ❖ Planetary Occultation Measurements.
 - ❖ What is Scintillation?
 - ❖ Interplanetary Scintillation (IPS) Telescopes/Arrays.
 - ❖ An Introduction to IPS and Basic IPS Theory.
- ❖ Some Recent IPS Results and LOFAR Technical Advances.
 - ❖ A Brief Introduction to IPS Three-Dimensional (3-D) Tomographic Reconstructions and Examples of their Usage.
- ❖ A Brief Introduction to Heliospheric Faraday Rotation (FR) and Initial Progress Towards Heliospheric FR Determination.
 - ❖ Lecture Summary.

A Brief Introduction to the Radio Spectrum!

The Electromagnetic (EM) Spectrum

- ❖ An overview of the EM spectrum; adapted from Heliophysics Volume 2, Chapter 4, by Tim Bastian.
- ❖ Commercial AM radio band lies in the LF-MF range, and the FM band lies in the VHF part of the spectrum.



The Radio Spectrum

Frequency Band Definition	Frequency Range	Wavelength Range	Band Designations
ELF - Extremely Low Frequency	< 300 Hz	> 1,000 km	-
ULF - Ultra Low Frequency	300 Hz - 3 kHz	1,000 km - 100 km	-
VLF - Very Low Frequency	3 kHz - 30 kHz	100 km - 10 km	-
LF - Low Frequency	30 kHz - 300 kHz	10 km - 1 km	-
MF - Medium Frequency	300 kHz - 3 MHz	1 km - 100 m	-
HF - High Frequency	3 MHz - 30 MHz	100 m - 10 m	-
VHF - Very High Frequency	30 MHz - 300 MHz	10 m - 1 m	-
UHF - Ultra High Frequency	300 MHz - 3 GHz	1 m - 100 mm	P (sometimes) = 300MHz - 1 GHz L = 1 GHz - 2 GHz
SHF - Super High Frequency	3 GHz - 30 GHz	100 mm - 10 mm	S = 2 GHz - 4 GHz C = 4 GHz - 8 GHz X = 8 GHz - 12 GHz Ku = 12 GHz - 18 GHz K = 18 GHz - 26 GHz
EHF - Extremely High Frequency	30 GHz - 300 GHz	10 mm - 1 mm	Ka = 26 GHz - 40 GHz Q = 30 GHz - 50 GHz U = 40 GHz - 60 GHz V = 50 GHz - 75 GHz E = 60 GHz - 90 GHz W = 75 GHz - 110 GHz F = 90 GHz - 140 GHz D = 110 GHz - 170 GHz

- ❖ An overview of the radio spectrum by band, frequency range, wavelength range, and band classification.

What is Occultation?

(Who can tell me?)

Solar Occultation During a Full Eclipse

- ❖ An occultation occurs when one object is hidden by another that passes between it and the observer; *i.e.* when an apparently larger body passes in front of an apparently smaller one.



- ❖ The total solar eclipse of 2006 clearly displaying the faint solar corona in all its glory. Image taken from Bisi, Ph.D. Thesis, 2006; courtesy of Dr. Richard A. Fallows (currently at ASTRON in The Netherlands).

Planetary Occultation Measurements.

Jupiter's Ionosphere

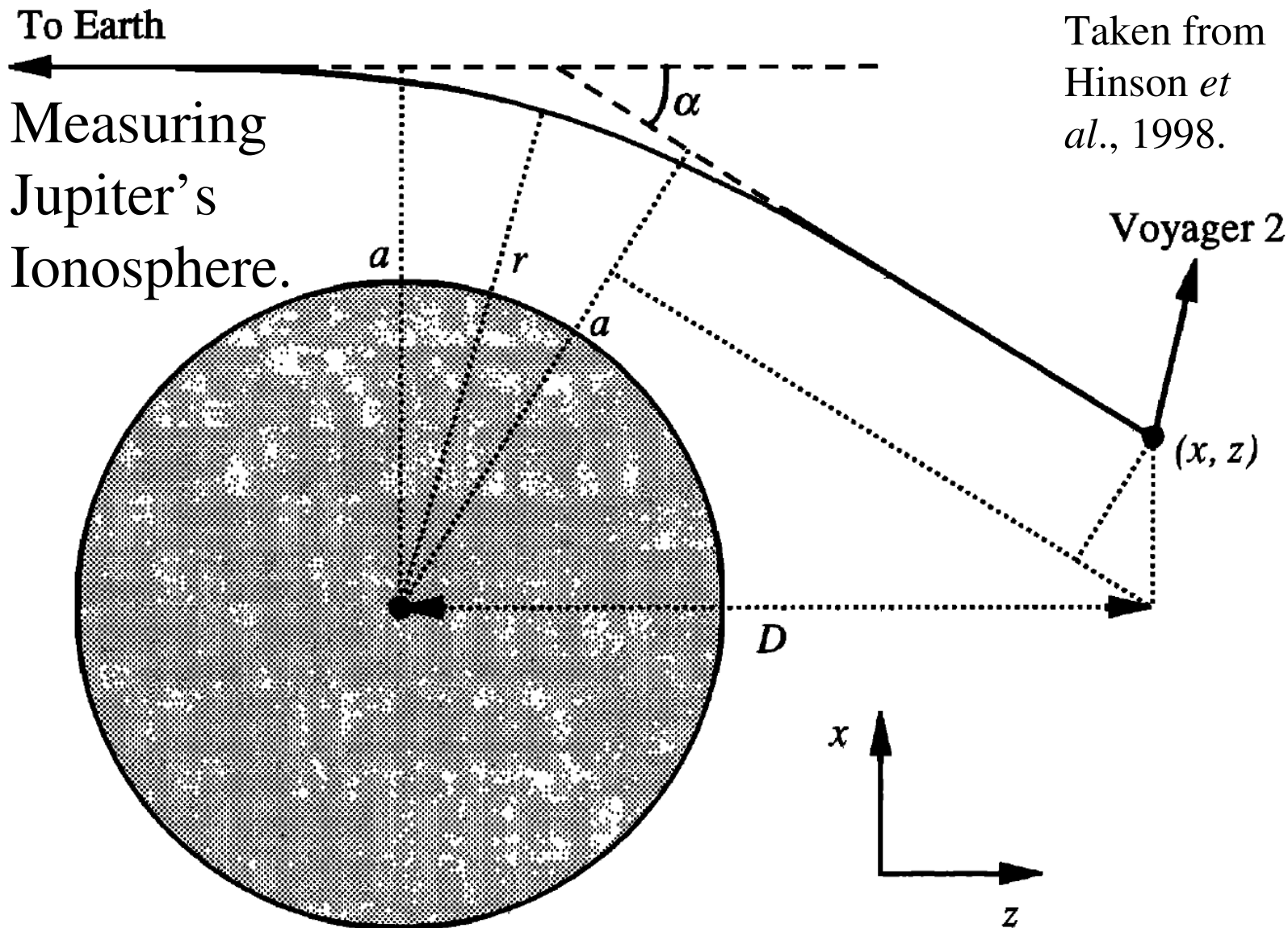


Figure 1. Schematic of Voyager 2 occultation by Jupiter. Solid line shows “ray path” followed by radio signals propagating from spacecraft to Earth. Impact parameter a , radius at ray periapease r , and spacecraft-to-planet distance D are measured from the local center of curvature of Jupiter, which is also the coordinate origin.

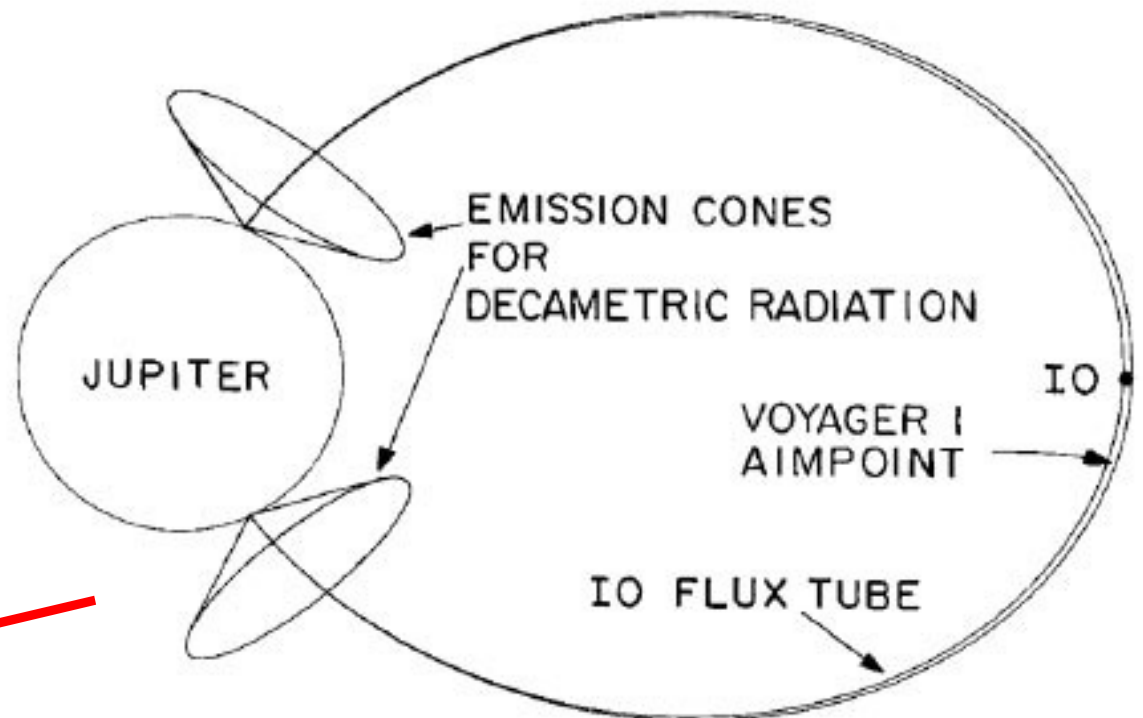
- ❖ The classical Doppler shift in signal radio frequency was measured which was caused by the refractive bending in Jupiter's atmosphere/ionosphere.

Jupiter and Io

❖ According to the literature, Io is acted upon by a $\mathbf{J} \times \mathbf{B}$ force which tends to try to propel it out of the Jovian system. In addition, its motion about Jupiter puts it through the Io plasma torus at Jupiter which carries two billion kilowatts of power into the Jovian ionosphere. The energy source for these processes is from Jupiter's relatively-fast rotation. This is an unusual planet-satellite coupling.

❖ Figure: The Io flux tube (IFT) and its associated decametric emission cones – to scale (Belcher, 1987).

❖ See Belcher, 1987 for further information.

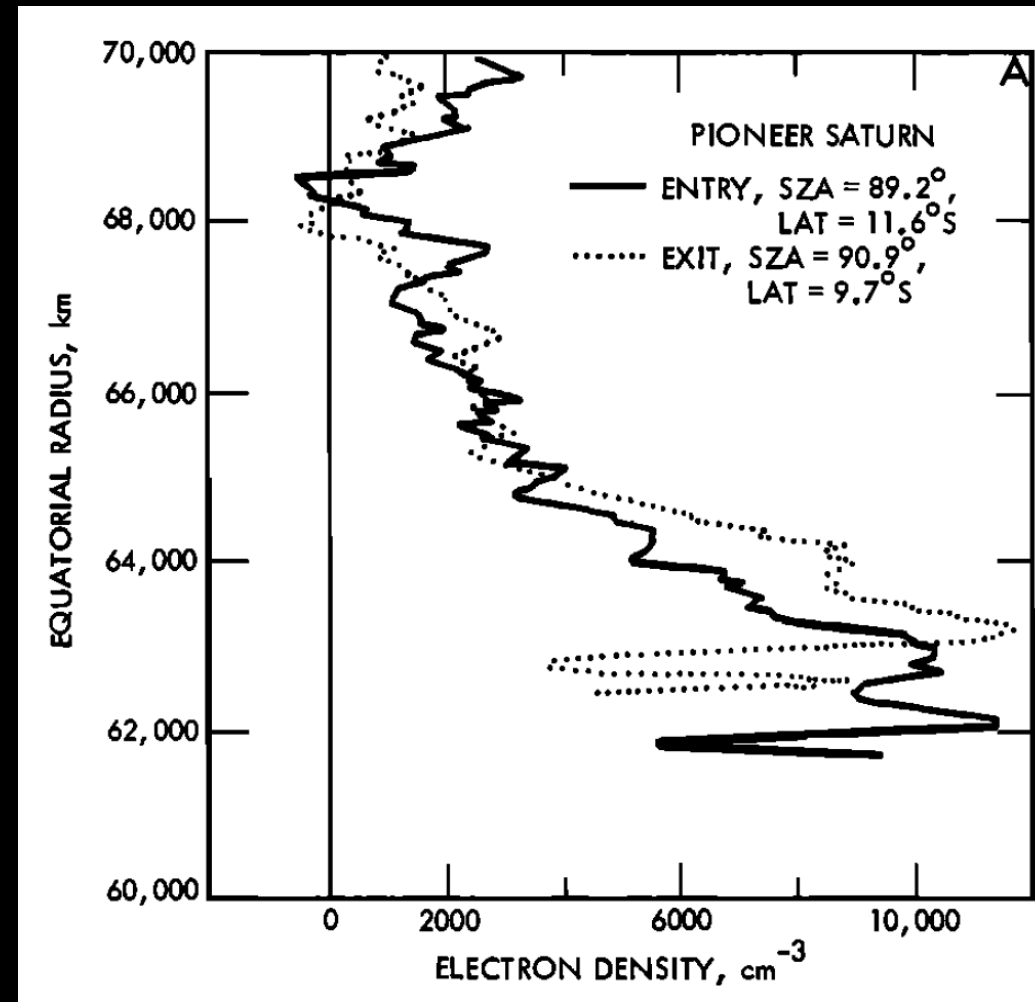


Jupiter and Callisto

- ❖ Electron density profiles were obtained at Callisto using data from the Galileo spacecraft with the radio occultation technique. There were five occultations by Callisto providing eight usable observing opportunities (entrance and exit observations).
- ❖ The detection of an ionosphere which was calculated as being generated by the photo-ionisation and electron-impact ionisation of the neutral gases at the surface.
- ❖ Detectable ionospheres were only when the side in which the moon is travelling (the ramside) was in sunlight which suggests the need for both photo-ionisation and the impact of a plasma onto the upper atmosphere of the moon.
- ❖ Results were obtained from the Galileo spacecraft; see Kliore *et al.*, 2002 for further information.

Saturn's Ionosphere and Atmosphere

- ❖ From radio occultation measurements of the Pioneer 11 flyby of Saturn on 01 September 1979, the ionosphere and upper atmosphere were measured.
- ❖ Revealed that the primary electron density peak of the ionosphere was at a height of 1,800 km with a density around $11,400 \text{ cm}^{-3}$.
- ❖ For further information, see Kliore, *et al.*, 1980 (figure also taken from here).



Saturn's electron density between equatorial radii of 60,000 km and 70,000 km. The solid curve is From entry data into occultation and the dashed curve is a profile obtained from exit data by using an artificial drift function; not to be used for magnitudes of electron density.

Saturn and Titan, and Venus' Ionosphere

- ❖ Saturn's largest moon, Titan, occulted a bright giant K-type star designated 28 Sgr on 03 July 1989.
- ❖ Strong scintillations were recorded in the stellar signal throughout the occultation which are attributed to the refractive-index changes in Titan's atmosphere (*e.g.* Hubbard *et al.*, 1988).
- ❖ An extensive discussion on this stellar occultation is given by Hubbard *et al.*, 1993.
- ❖ Initial observations of the night-side ionosphere of Venus were possible through radio-occultation measurements with the Pioneer Venus Orbiter Spacecraft. See Kliore *et al.*, 1979.
- ❖ What about the Earth...

Earth's Atmosphere: GPS Radio Occultations

From Kursinski *et al.*, 1997.

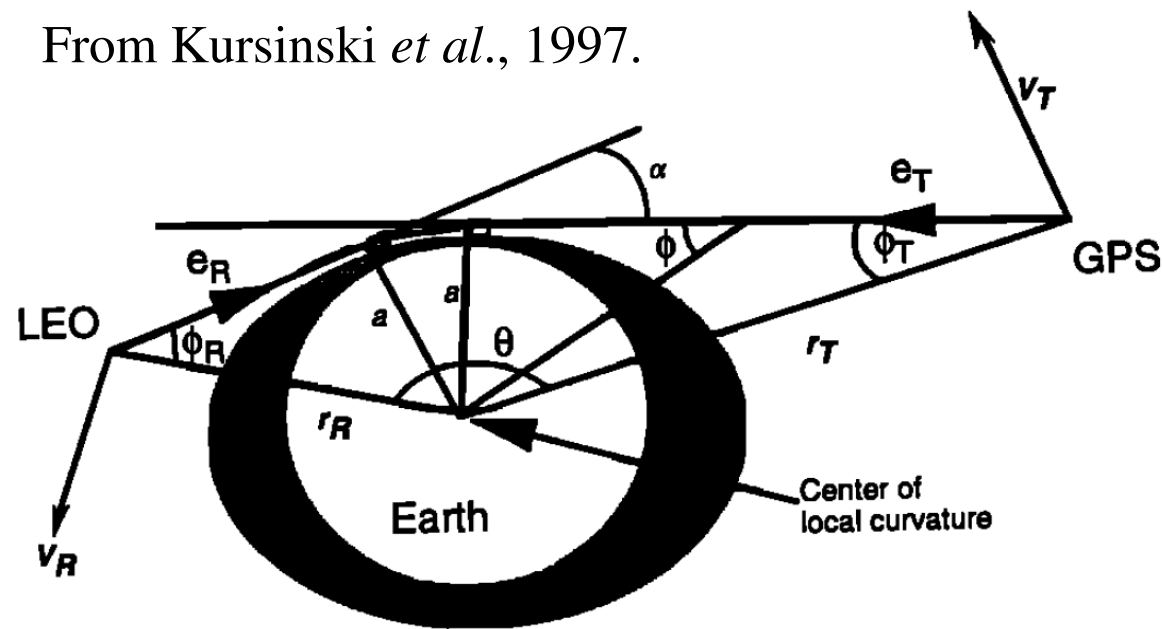


Figure 1. Instantaneous occultation geometry for the Global Positioning System (GPS) and low Earth orbiter (LEO) satellites defining variables for the derivation of α and a from Doppler shift, spacecraft position, and spacecraft velocity measurements.

- ❖ Allows for the derivation of atmospheric profiles.
- ❖ Momentum and energy within the atmosphere is transported by small-scale waves which contribute to the middle atmospheric structure and circulation – the height is important.

❖ Radio occultation observations provide a high vertical resolution measure and sensitivity to density and temperature perturbations (from waves) and turbulence used to characterise properties in the atmospheres of Venus, Jupiter, Titan, Uranus, and Neptune. See Kursinski *et al.*, 1997 and references therein, for further details.

What is Scintillation?

(Again, who can tell me?)

Scintillation and Quasars

- ❖ George Gamow, “Quasar”, 1964.

Twinkle, twinkle quasi-star
Biggest puzzle from afar
How unlike the other ones
Brighter than a billion suns.
Twinkle, twinkle quasi-star
How I wonder what you are.

- ❖ Quasar 3C 273 as imaged by the Hubble Space Telescope's Advanced Camera for Surveys.

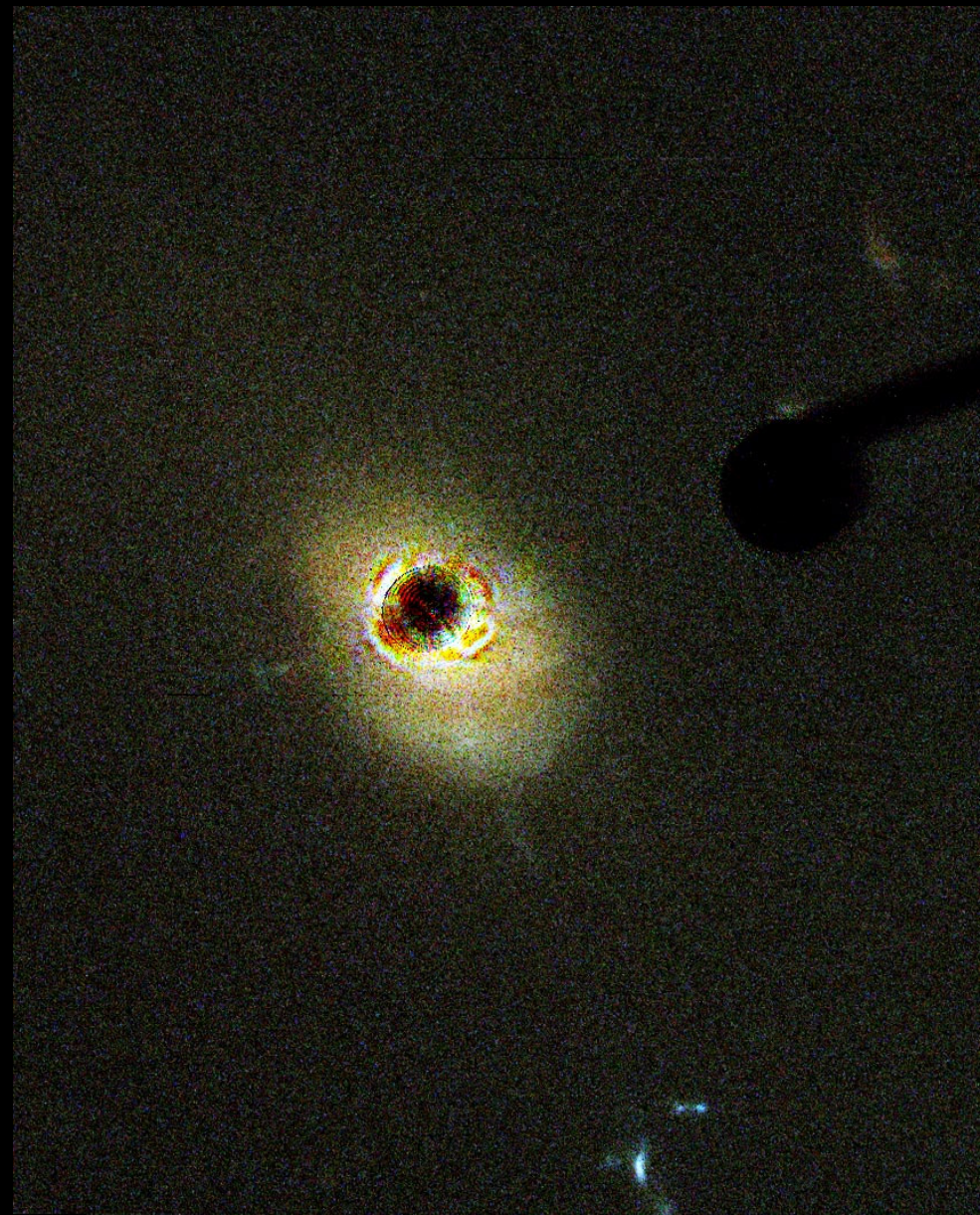


Image is courtesy of NASA, A. Martel (JHU), H. Ford (JHU), M. Clampin (STScI), G. Hartig (STScI), G. Illingworth (UCO/Lick Observatory), the ACS Science Team and ESA.

Interplanetary Scintillation (IPS)

Telescopes/Arrays

EISCAT, ESR, and MERLIN (224 MHz-~6GHz)



Above: The European Incoherent SCATter radar (EISCAT) and EISCAT Svalbard Radar (ESR) radio telescopes from left-to-right: Tromsø, Norway (M.M. Bisi, October 2003); Kiruna, Sweden (M.M. Bisi, May 2003); Sodankylä, Finland (<http://www.eiscat.com/sodan.html>); and the ESR 42m in the foreground and steerable 32m in the background (M.M. Bisi, May 2005).



Left: The Multi-Element Radio-Linked Interferometer Network (MERLIN) MkIa (Lovell) radio telescope at Jodrell Bank (near Manchester, England); and Right: The MERLIN MkII radio telescope also at Jodrell Bank (M.M. Bisi, May 2004).



The LOW Frequency ARray (LOFAR) (1)



LOFAR superterp (top) and
LOFAR Chilbolton (bottom).



LOFAR Core High-Band Antenna (top) and
LOFAR Core Low-Band Antenna (bottom);
both with Dr. Richard A. Fallows
(~ 5' 5½" tall) in for size comparison.



LOFAR core in The Netherlands with stations around The Netherlands and International Stations in Germany (5), France (1), Sweden (1) and in the UK (1). The stations shown in green are complete and operational while yellow depicts stations that are under construction as of March 2013.

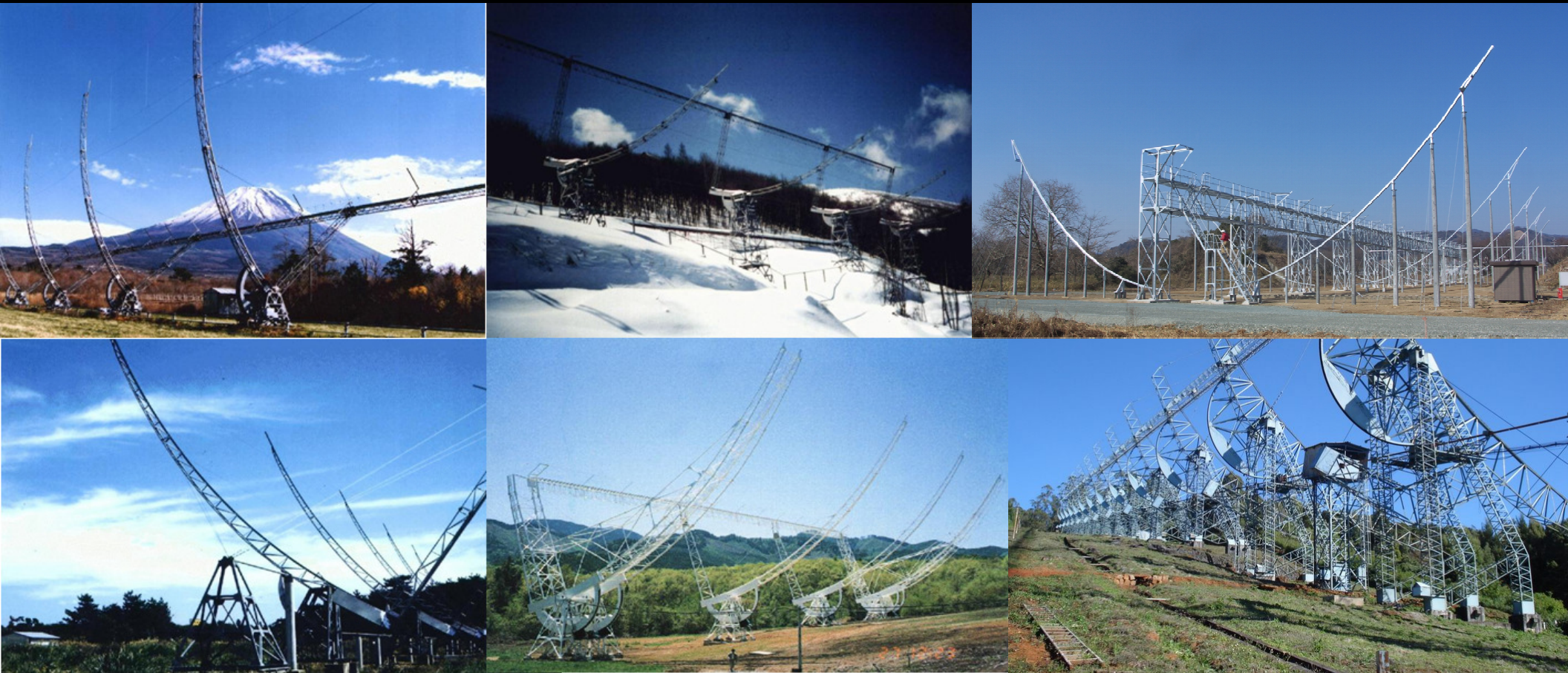
LOFAR (2)



LOFAR (3)

- ❖ Frequency agile system over two primary observing bands of 10 MHz to ~240 MHz split into 10 MHz to 90 MHz (LBA) and 110 MHz to ~240 MHz (HBA) with two antenna types.
- ❖ Ample collecting area with plenty of combinations of multi-site observations with the International Stations over long baselines.
- ❖ Experimentation with beam modes to enable band widths encompassing 80 MHz to ~the entire observing frequency range!
- ❖ Possibilities of $\sim 5^\circ$ angular resolution in three-dimensional (3-D) tomographic reconstructions look plausible with LOFAR data.
- ❖ The Murchison Widefield Array (MWA) in Western Australia could match (or possibly exceed) the number of observations per day but will not offer the multi-site observations of LOFAR.
- ❖ Kilpisjärvi Atmospheric Imaging Receiver Array (KAIRA) based on LOFAR technology located just inside Finland.

Japan, India, and other IPS Arrays/Telescopes



The Solar Terrestrial Environment Laboratory (STELab) antennas of Fuji (top left), Sugadaira (top middle), (new) Toyokawa (top right), (old) Toyokawa (bottom left), and Kiso (bottom middle); and the Ootacamund (Ooty) Radio Telescope (ORT) (bottom right)
(Courtesy of http://stesun5.stelab.nagoya-u.ac.jp/uhf_ant-e.html, B.V. Jackson, and P.K. Manoharan).

Others also include: MEXART, Mexico; Pushchino, Russia; UTR-2, Ukraine; and the Murchison Widefield Array (MWA), Australia.

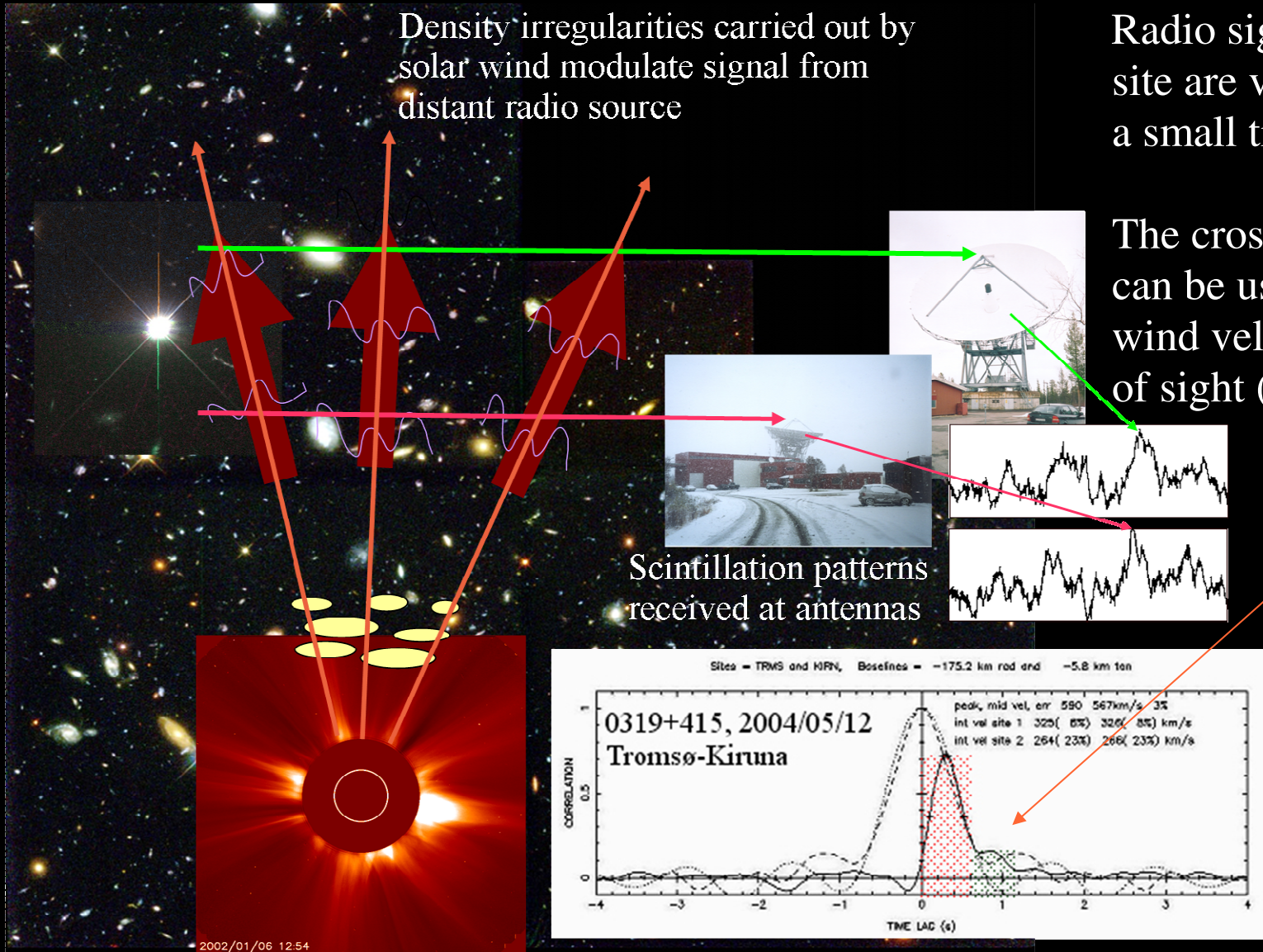
**An Introduction to IPS
and Basic IPS Theory.**

An Introduction to IPS (1)

Density irregularities carried out by solar wind modulate signal from distant radio source

Radio signals received at each site are very similar except for a small time-lag.

The cross-correlation function can be used to infer the solar wind velocity(s) across the line of sight (LOS).



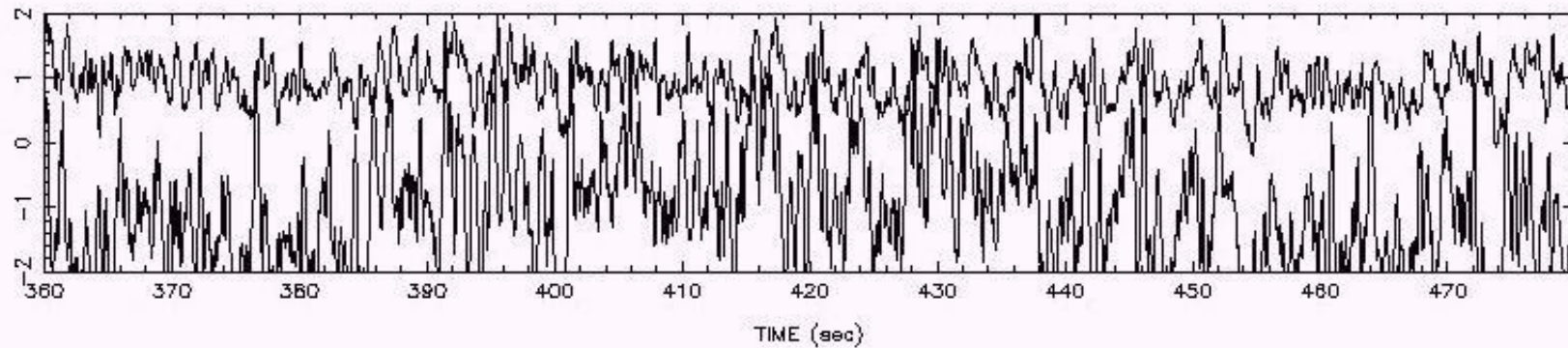
(Not to scale)

Hubble Deep Field – HST (WFPC2) 15/01/96 – Courtesy of R. Williams and the HDF Team and NASA

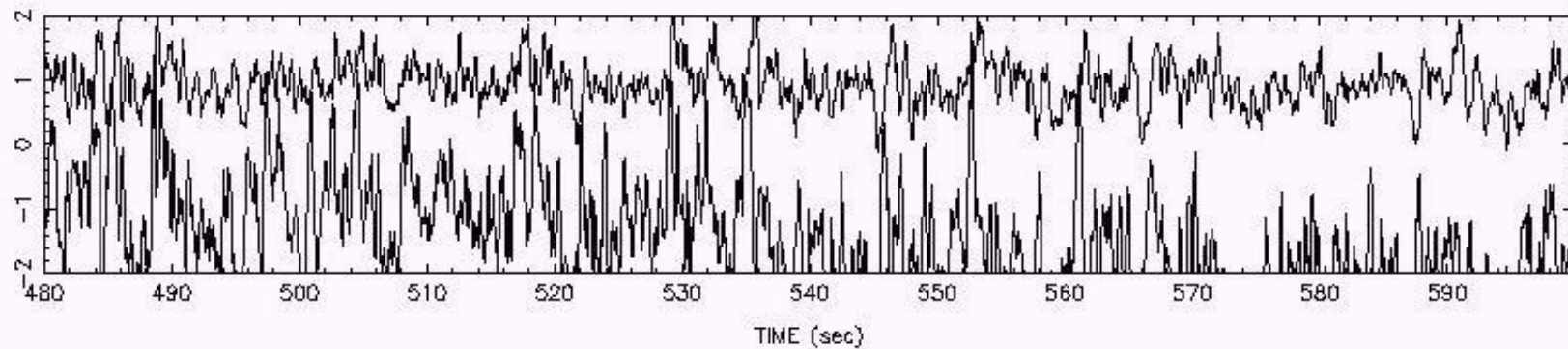
IPS is most-sensitive at and around the P-Point of the LOS to the Sun and is only sensitive to the component of flow that is perpendicular to the LOS; it is variation in intensity of astronomical radio sources on timescales of ~ 0.1 s to ~ 10 s that is observed.

An Introduction to IPS (2)

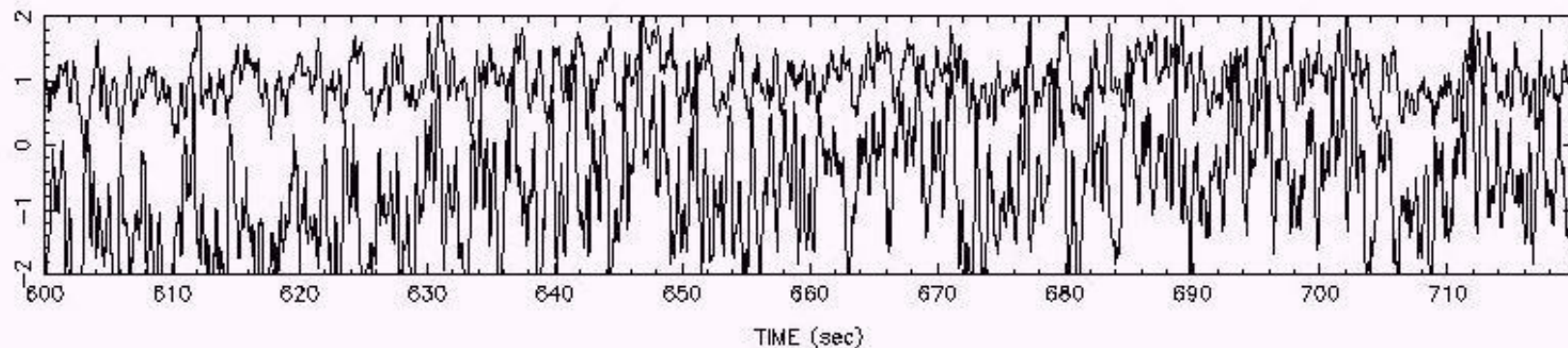
s=start f=end x=delete q=done r=reject c=threshold clip p=replot 1229+020 ON 980911 AT 90800 BOT-TOP KIRN SDKY



s=start f=end x=delete q=done r=reject c=threshold clip p=replot 1229+020 ON 980911 AT 90800 BOT-TOP KIRN SDKY



s=start f=end x=delete q=done r=reject c=threshold clip p=replot 1229+020 ON 980911 AT 90800 BOT-TOP KIRN SDKY



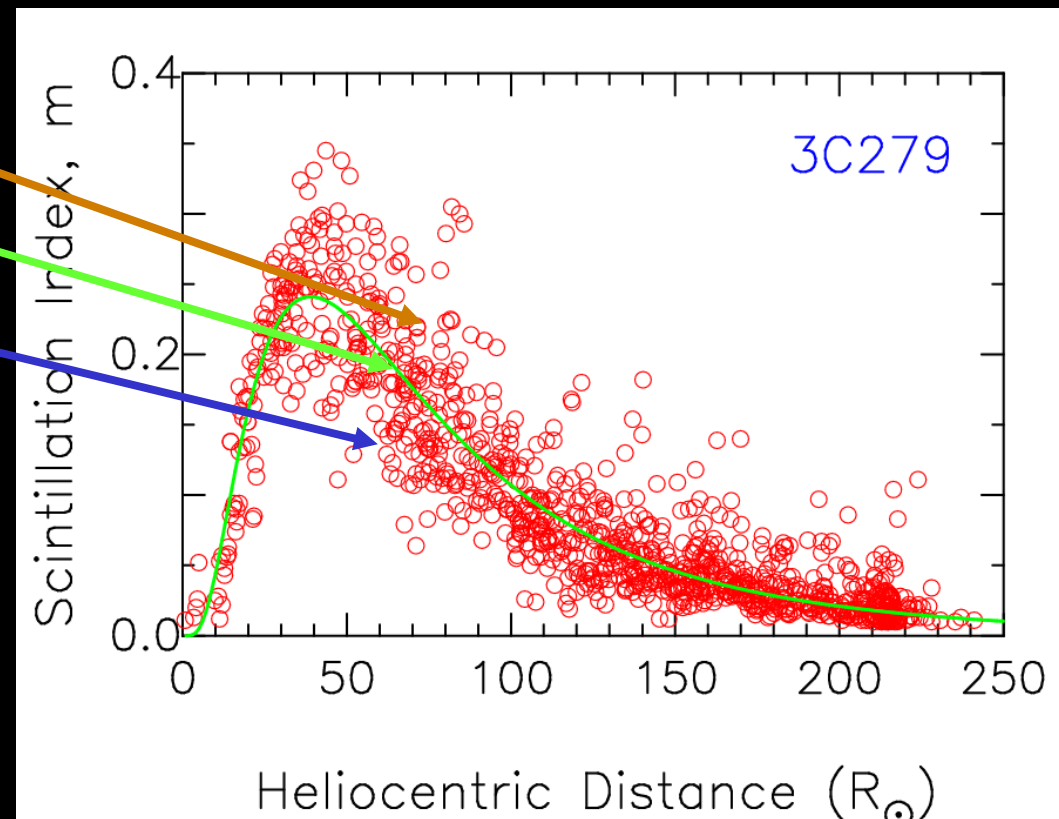
An Introduction to IPS (3)

Density Turbulence

- ❖ Scintillation index, m , is a measure of level of turbulence.
- ❖ Normalized Scintillation index, $g = m(R) / \langle m(R) \rangle$.

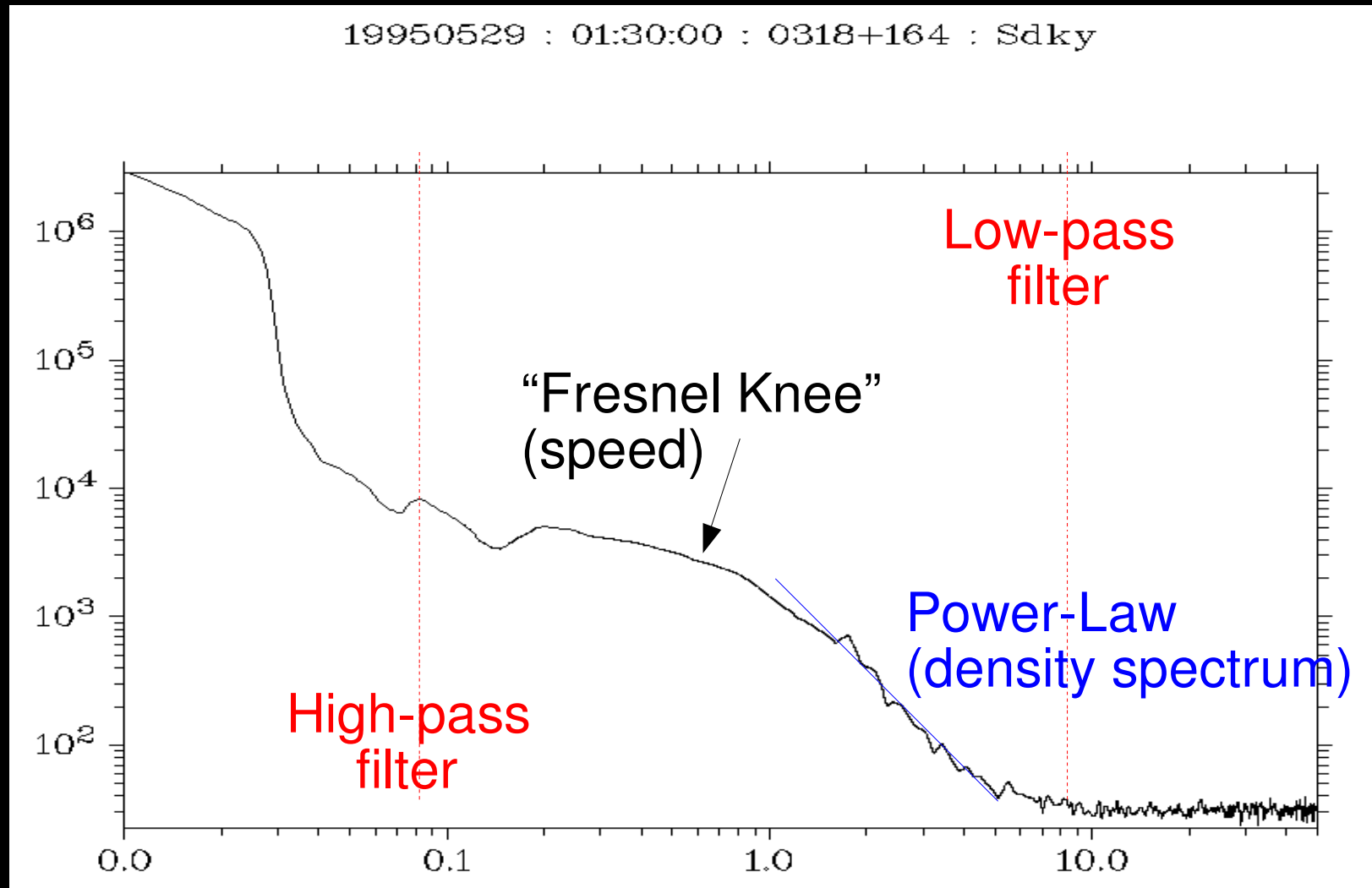
- $g > 1 \rightarrow$ enhancement in δN_e .
- $g \approx 1 \rightarrow$ ambient level of δN_e .
- $g < 1 \rightarrow$ rarefaction in δN_e .

(Courtesy of
Prof. P.K. Manoharan.)



Scintillation enhancement with respect to the ambient wind identifies the presence of a region of increased turbulence/density and possible CME along the line-of-sight to the radio source.

An Introduction to IPS (4)



An example power spectrum from an observation of IPS with its key features marked.

- Plot courtesy of Dr. Richard A. Fallows, ASTRON, The Netherlands.

An Introduction to IPS (5)

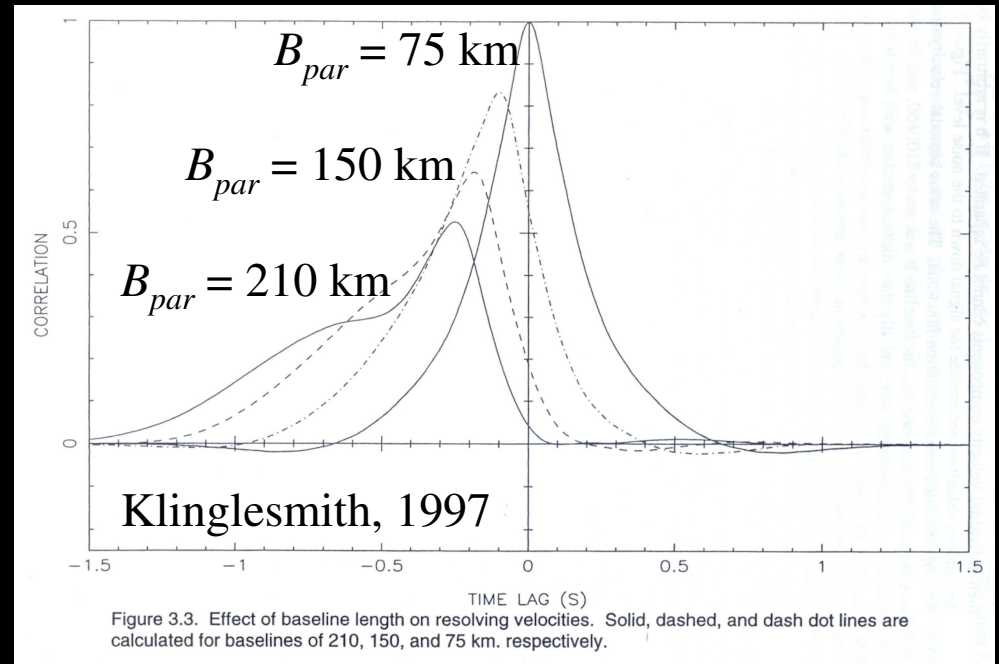
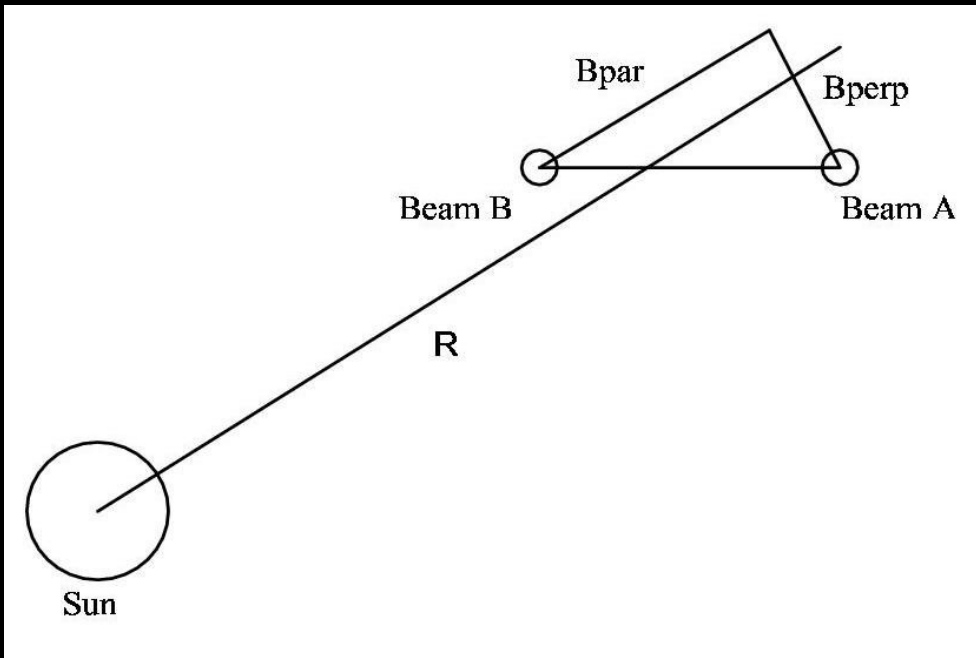


Figure 3.3. Effect of baseline length on resolving velocities. Solid, dashed, and dash dot lines are calculated for baselines of 210, 150, and 75 km, respectively.

- ❖ The ability to distinguish between streams of different velocity improves as the parallel baseline length (B_{par}) increases between two observing sites; if (B_{par}) is long enough, streams with different velocities appear as widely-separated peaks in the (temporal) cross-correlation function.
- ❖ The height of the maximum cross correlation decreases as parallel baseline length increases since density pattern changes with time.

Basic IPS Theory

- Hewish, A., “A user's guide to scintillation”, Journal of Atmospheric and Terrestrial Physics, 51, pp.743-750, 1989.

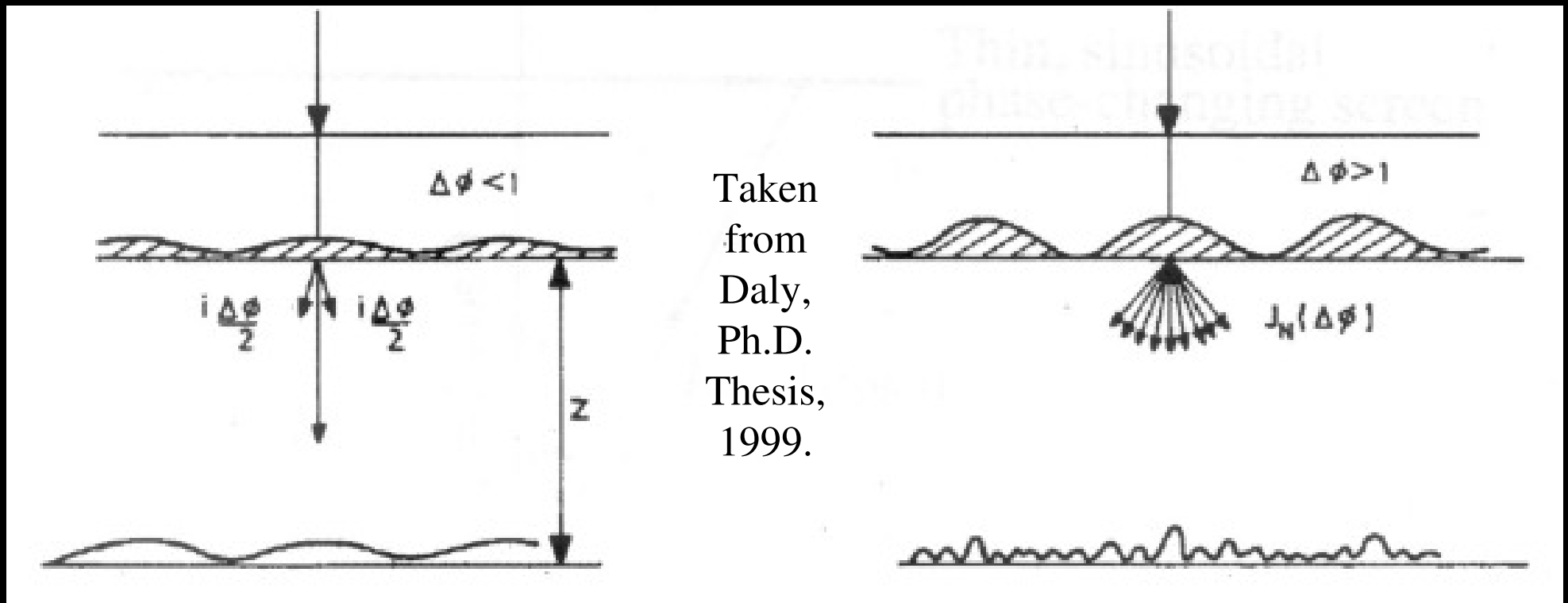
Abstract:

Scintillation methods and the theory underlying scintillation methods are reviewed. Consideration is given to diffractive and refractive scintillation and describing irregular media. Application of scintillation are discussed, including ionospheric, interplanetary, and interstellar scintillation and scintillation and source size.

Basic IPS Theory (1)

- ❖ Distant, compact, astronomical radio source observed at frequency f – assume plane incident waves on the solar wind; and assume all source power is in a single point.
- ❖ Consider scattering by a single thin screen: assume solar wind varies in density by δN around mean density $\langle N \rangle$.
- ❖ Mean refractive index (from Maxwell): $n = 1 - f_p^2/2f^2$.
- ❖ Variation in refractive index: $\delta n = \delta N e^2 / (8\pi^2 \epsilon_0 m_e f^2)$; provided that $f \gg$ plasma frequency f_p .
- ❖ The phase variation in a scattered wave in the solar wind can be assumed to a 1st approximation that $\delta N \propto N^2$.
- ❖ The phase variation between different parts of scattered waves increases as N increases, and decreases as f increases.
- ❖ Next, consider the effect of a single thin screen in which the electron density varies sinusoidally (with wavenumber K)...

Basic IPS Theory (2)

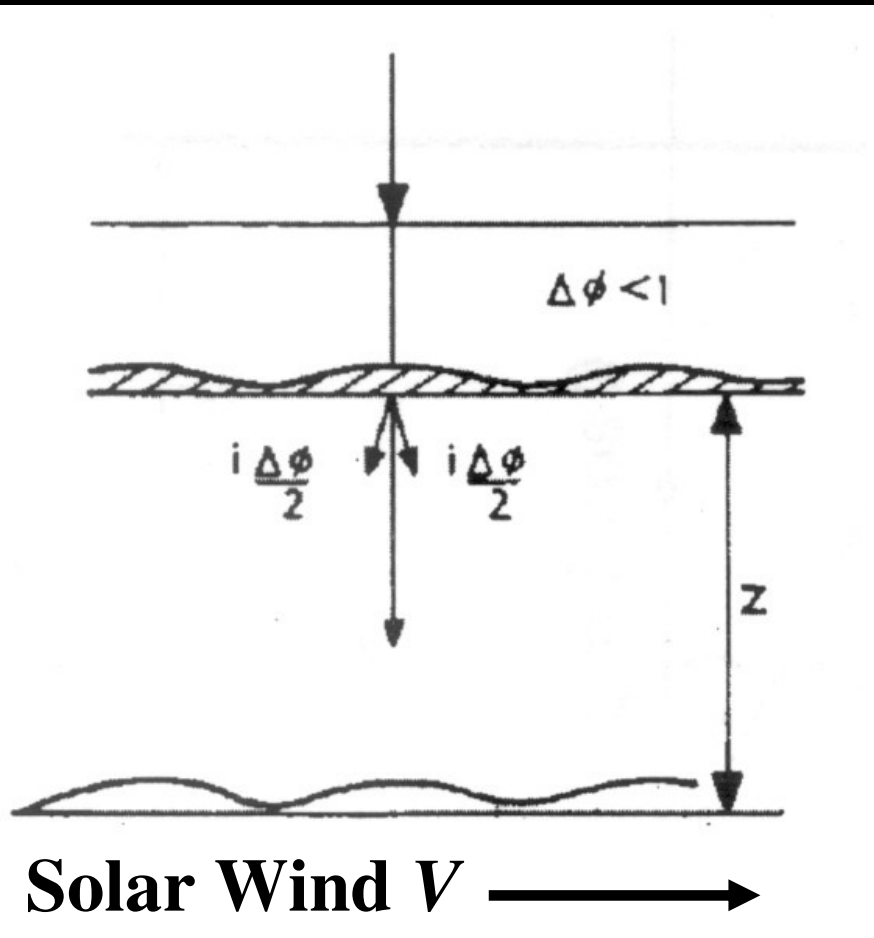


- ❖ An incident plane wave (wavenumber k) falling onto the x-plane.
- ❖ Figure shows the scintillation by a sinusoidal phase-changing screen: “weak scattering” (left) $\Delta\phi \ll 1$ radian, and “strong scattering” (right) $\Delta\phi \gg 1$ radian; IPS becomes very complex in strong scattering and generally only when the weak-scattering regime applies do we use results from observations of IPS.

Basic IPS Theory (3)

- ❖ Providing the maximum variation in phase $\Delta\phi \ll 1$ radian (*i.e.* within the weak-scattering regime), the effect of the screen is to introduce a pair of additional waves (of complex amplitude $i\Delta\phi/2$) propagating at angles of $\theta = \pm \sin^{-1}(K/k)$ to the “average” wave.
- ❖ If $K \ll k$, that is, the scattering screen wavelength is much greater than the wavelength of the incident radio waves: $\theta = \pm(K/k)$.
- ❖ If the waves come from a point source at infinite distance, then an observer looking through the screen from close to it would see the source flanked by a pair of weak images displaced by θ from it.
- ❖ The diffraction pattern (in intensity, or amplitude) across any plane “below” the screen “will result from the mutual interference of the three waves and will exhibit sinusoidal variations in amplitude and phase with wavenumber K ” (Hewish, 1989).
- ❖ Thus, the diffraction pattern has same scale as a refracting screen.

Basic IPS Theory (4)



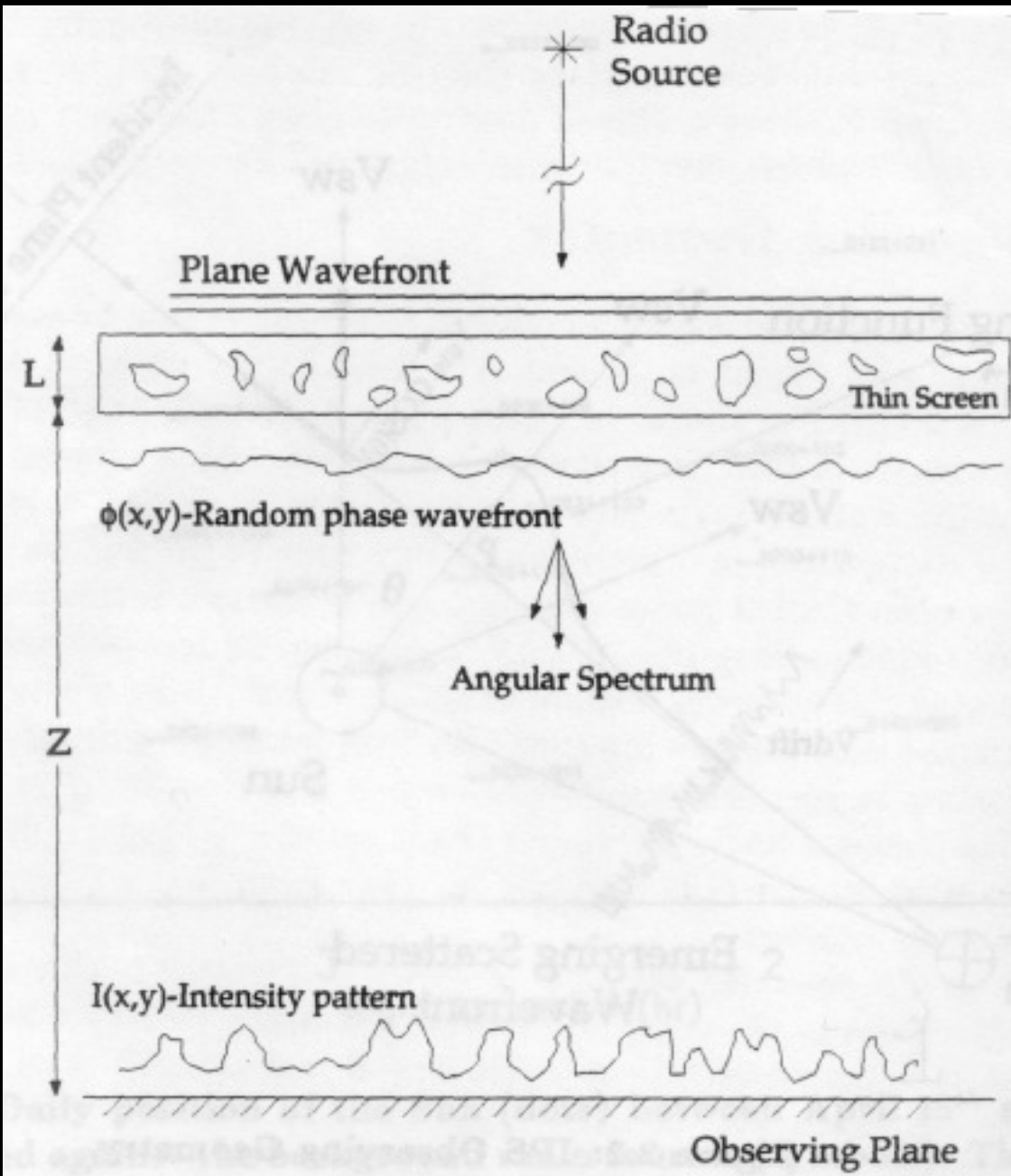
- ❖ Staying with the single sinusoidal scattering screen, then the screen has wavenumber K , and wavelength: $\lambda = 1/K$.
- ❖ If screen is moving across the ray path for the observation at speed V , then the diffraction pattern will also be moving across a receiver “below” the screen at speed V .

- ❖ The receiver will record a time-varying intensity with peaks every $1/KV$ seconds.
- ❖ Observing the same source with two telescopes means the time difference at which peaks are observed can be used to determine V , which together with the time interval between peaks gives K .

Basic IPS Theory (5)

- ❖ However: the turbulence in the solar wind is not a simple, single, sinusoidal screen, and real radio sources are compact but rarely perfectly point-like.
- ❖ So, the next step is to look at a compact radio source as viewed through a screen which has random phase changes.
- ❖ For weak scattering, the spatial scale of fluctuations cast by the phase-changing screen is the same as the spatial scale of the irregularities in the screen.
- ❖ Phase change along path L through screen: $\theta = 2\pi/\lambda \int^L n dz$; then the thin diffraction screen imparts random phase variations to the emerging wavefront (amplitude initially unchanged).
- ❖ As the wavefront continues in the z direction, the interference leads to the formation of a spatial intensity pattern.

Basic IPS Theory (6)



- ❖ At low frequencies and in the weak-scattering limit, the intensity spectrum reduces to the phase spectrum multiplied by the Fresnel filter.
- ❖ The physical conditions for this case are that the scattered waves interfere only with the unperturbed (bulk-refracted) incident wave and not with themselves.

Basic IPS Theory (7)

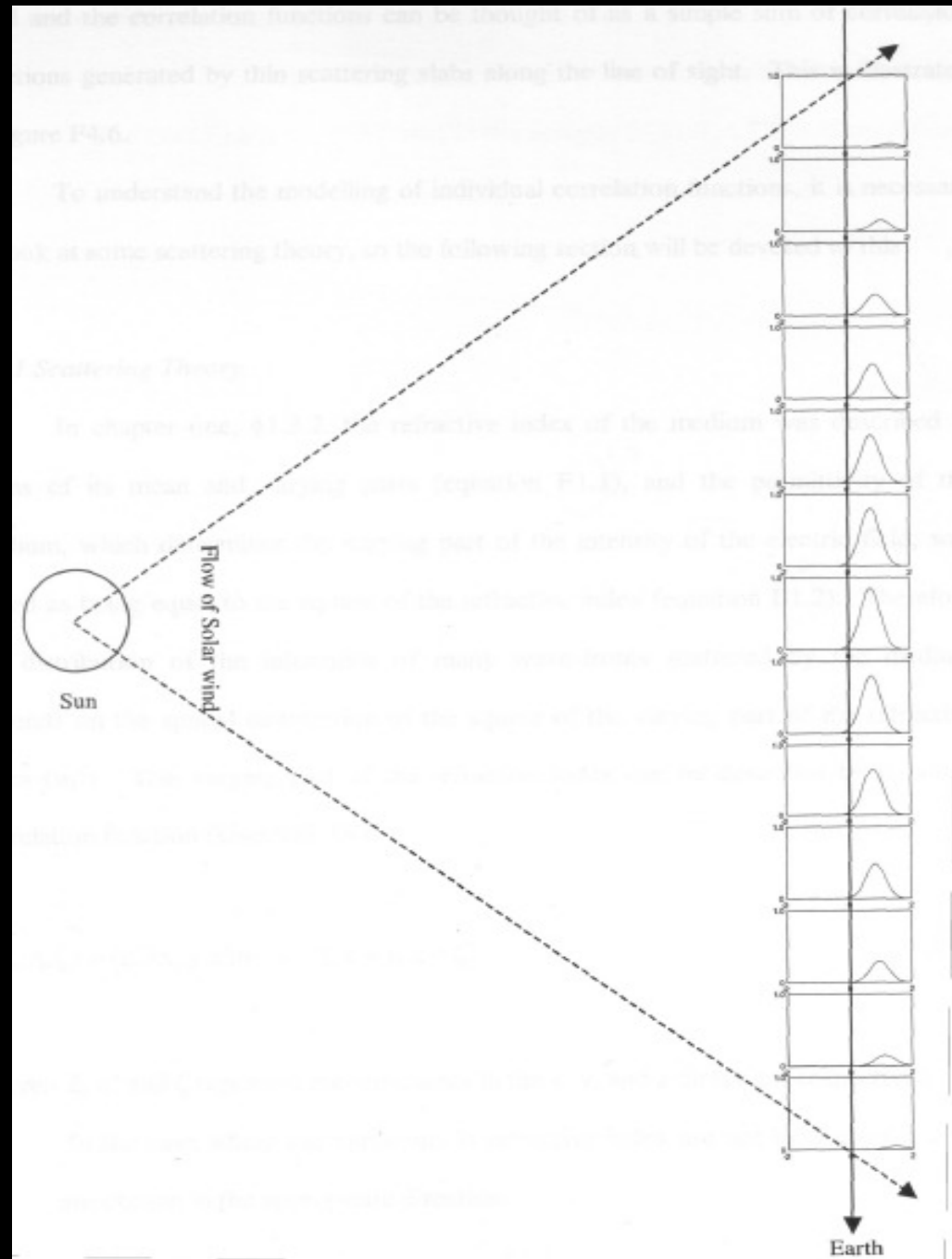
- ❖ At low frequencies and in the weak scattering limit: the intensity spectrum $P_{\Delta I(K)} = 4\sin^2(K^2 z/2k)P_{\varphi(K)}$, where $P_{\varphi(K)}$ is the phase spectrum which follows the spectrum of refractive index.
- ❖ If the scattering screen, and thus the resulting intensity pattern itself, drifts across the ray path, then it will be observed as a time series in signal power (*i.e.* as amplitude variations).
- ❖ The solar wind is a three-dimensional (3-D) structure, so radio waves from a distant compact radio source have passed through many scattering screens on their way from the source to where they are detected at the receiver.
- ❖ The assumption that the scattered waves interfere only with the unperturbed (bulk-refracted) incident wave and not with themselves is known as the Born approximation.

Basic IPS Theory (8)

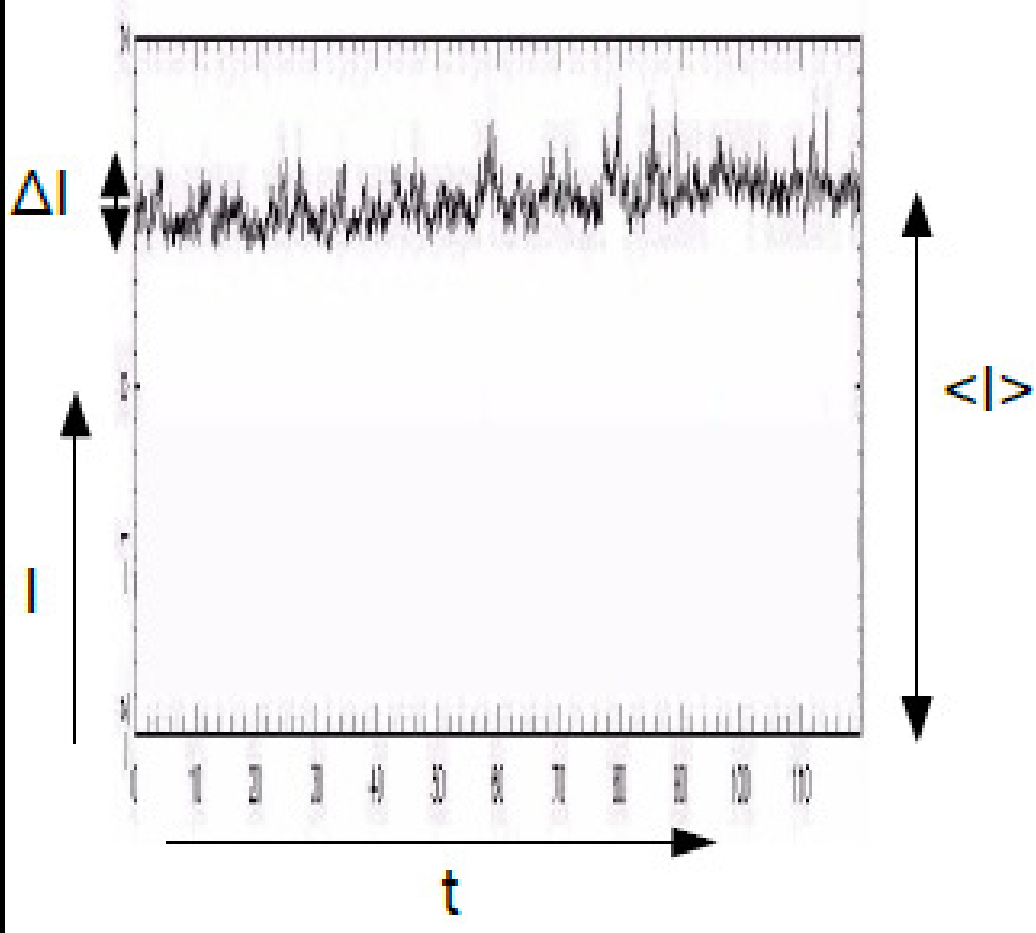
- ❖ In weak scattering along with the Born approximation, the results of scattering from each individual screen can be treated independently of each other.
- ❖ Thus, the intensity pattern observed at the receiver is the linear sum of the intensity patterns generated by all scattering events along the ray path; this does NOT hold true for strong scattering.
- ❖ The ray path passes through extended regions of the solar atmosphere (solar wind structure) and properties of solar wind may (and indeed will) differ greatly.
- ❖ The ray path is nearest to the Sun near its “centre” and furthest away at the ends.
- ❖ The near-Earth regions of the ray path may not show fully-developed intensity variations.

Basic IPS Theory (9)

- ❖ This leads to the observed intensity spectra; correlation functions are weighted sums of spectra/correlation functions cast by each of the scattering events.
- ❖ We can (in principle) take account of weighting and reconstruct properties of each scattering screen from the observed intensity spectra and/or correlation functions.



Basic IPS Theory (10)



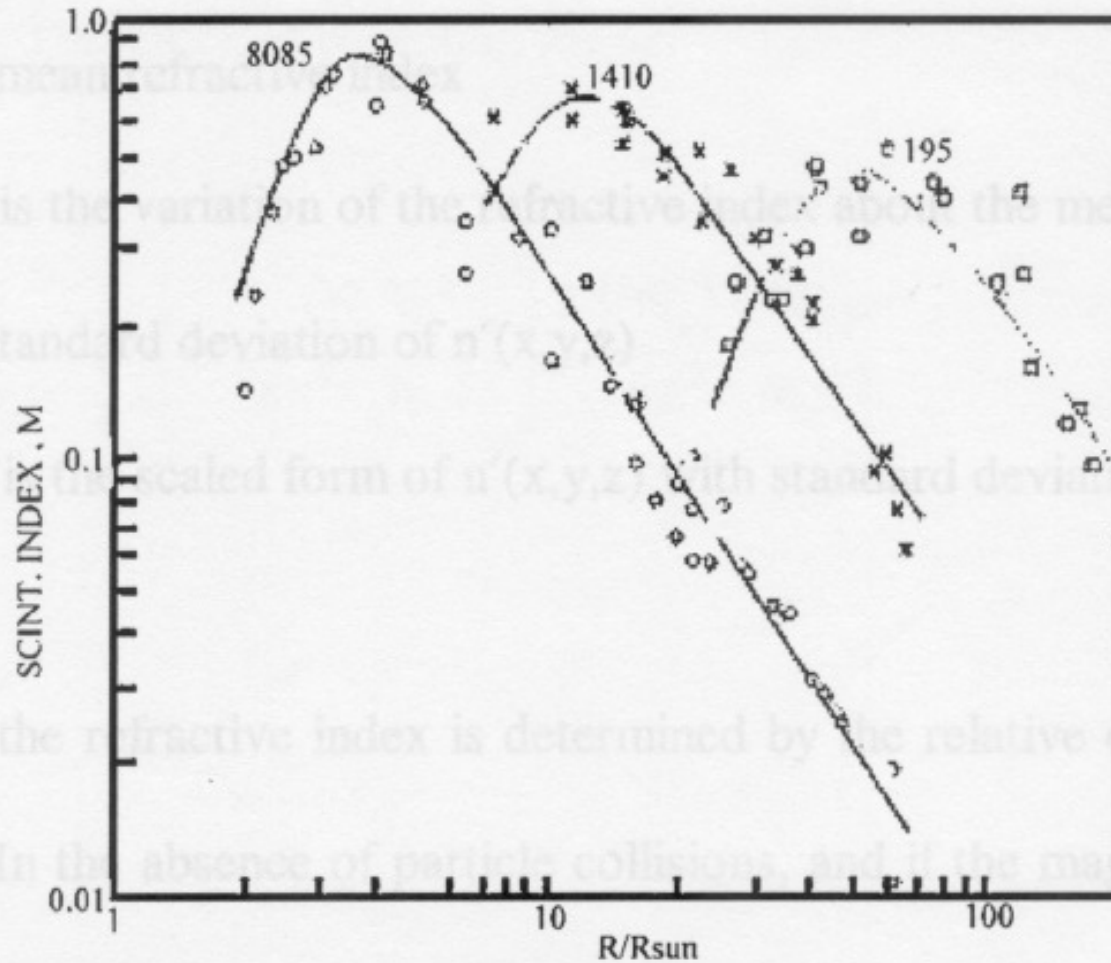
❖ The degree of variation of intensity seen in a time series generally expressed as scintillation index, m , as:

$$m^2 = \langle (I(t) - \langle I \rangle)^2 \rangle / \langle I \rangle^2,$$

where $I(t)$ is the source intensity observed at time t , and $\langle I \rangle$ is the average source intensity over the observation.

❖ The value of the scintillation index depends principally upon: the distance from the Sun (refractive index and thus phase variation); the source structure (at 928 MHz, sources wider than $\sim 0.5''$ do not scintillate); the observing frequency; and the solar-wind density.

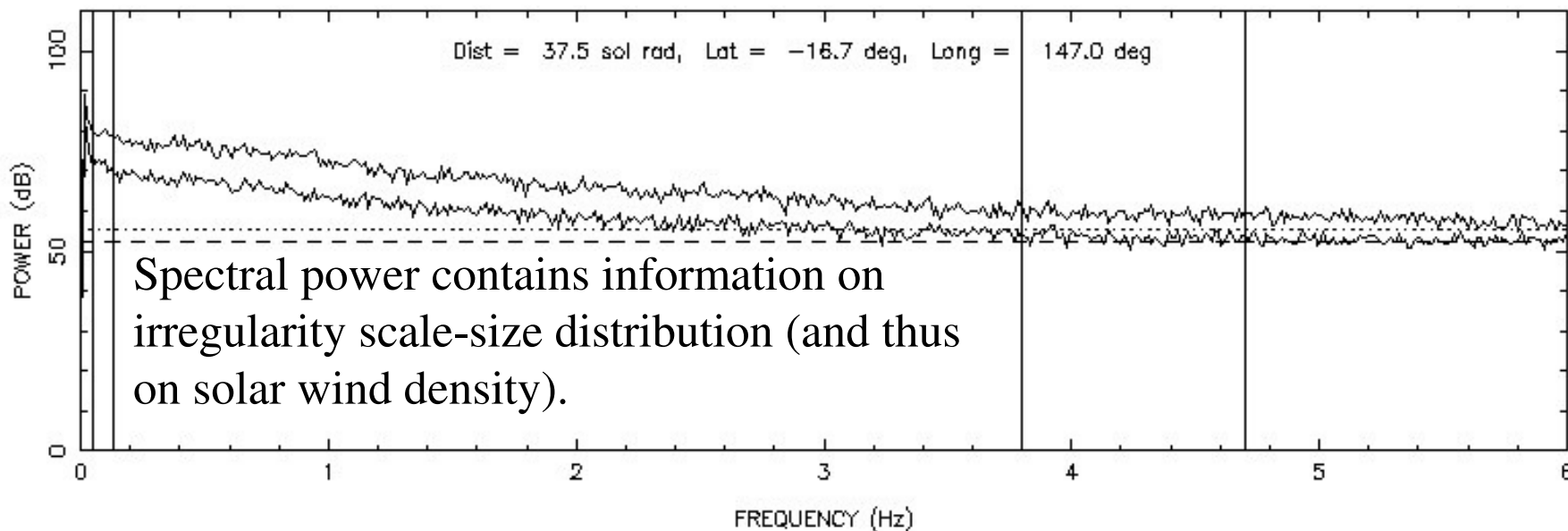
Basic IPS Theory (11)



Scintillation index versus distance from the Sun for three different observing frequencies (after Coles 1978). The sources used are 3C279 at 8085MHz and 1410MHz; and 3C138 at 195MHz.

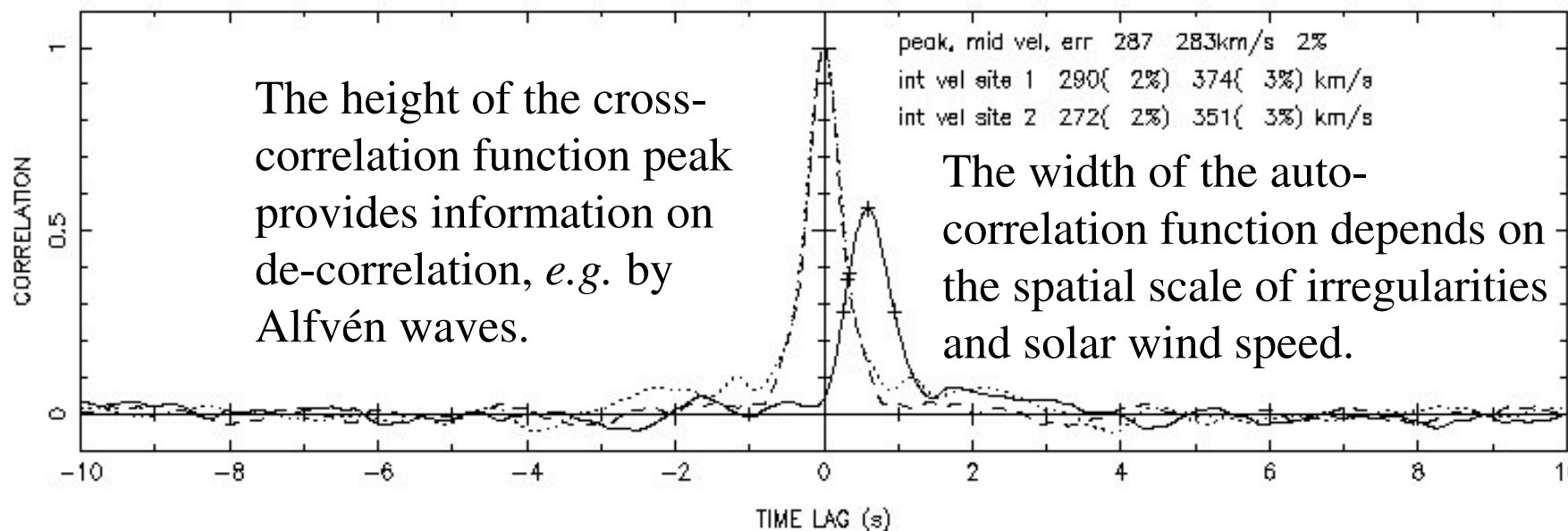
Basic IPS Theory (12)

EISCAT IPS ***** at 33100 UT Source = 0318+164



The time lag for the peak of the cross-correlation function gives information on the solar-wind outflow speed and the 1/2 power time lags (skew of function) provide information on the spread in velocity(s).

Sites = TRMS and KIRN, Baselines = -187.4 km rad and -41.8 km tan



Basic IPS Theory (13)

$$P(f) = 8\pi^2 r_e^2 \lambda_1 \lambda_2 \int_0^\infty \frac{2\pi}{v_p(z)} \int_{-\infty}^\infty \sin\left(\frac{q^2 \lambda_1 z}{4\pi}\right) \sin\left(\frac{q^2 \lambda_2 z}{4\pi}\right) |V(q, z, \theta_0)|^2 q^{-\alpha} \exp\left[-\left(\frac{q}{q_i}\right)^2 R^{-4}\right] dq_y dz$$

(Fallows *et al.*, 2006)

IPS Power Spectrum.

r_e is the classical electron radius;

λ is the observing wavelength;

α is the power law exponent, e.g. Kolmogorov;

v_p is the component of solar wind velocity perpendicular to the line of sight;

q is the 2-dimensional spatial wavenumber (normally in x-y coordinates);

q_i is the inner-scale for turbulence (the scale at which the turbulence dissipates);

z is the distance from Earth to the scattering “screen”;

θ_0 is the diameter of the source in radians;

and $V(q, z, \theta_0)$ is the visibility function of a radio source.

(Taken from:
Bisi, Ph.D.
Thesis, 2006.)

$$\text{Fresnel Filter} = 4 \sin^2\left(\frac{q^2 \lambda z}{4\pi}\right)$$

Single-frequency
IPS by example.

$$q_f = \sqrt{\frac{4\pi}{\lambda z}}$$

Dual-frequency IPS.

- ❖ The Fresnel filter acts as a high-pass filter attenuating wave-numbers below the Fresnel spatial frequency, q_f . For observing frequencies of 1,420 MHz (~21 cm)/928 MHz (~32 cm)/500 MHz (~60 cm), the maximum scale-size of irregularities at a “thin screen” of scattering at 1AU distance from the Earth is ~177 km/~219 km/~300 km, respectively.

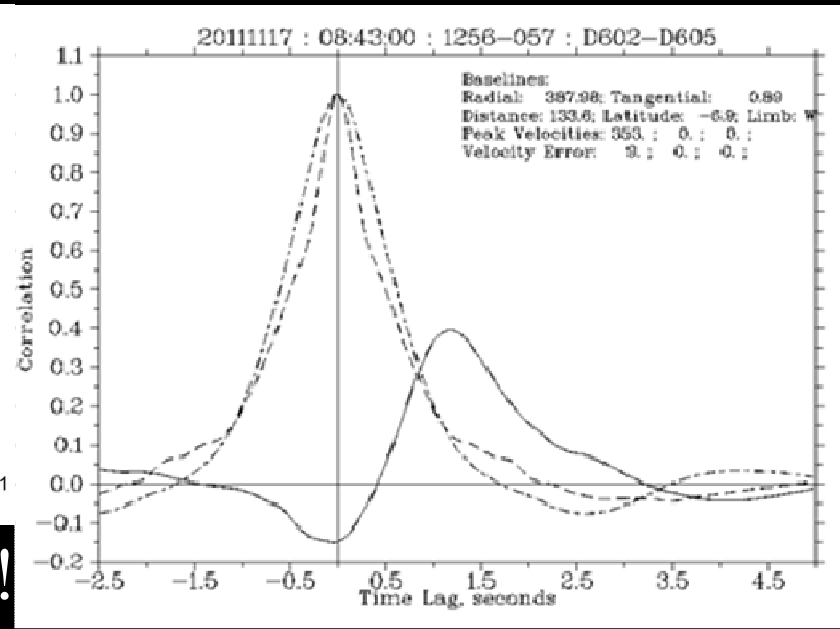
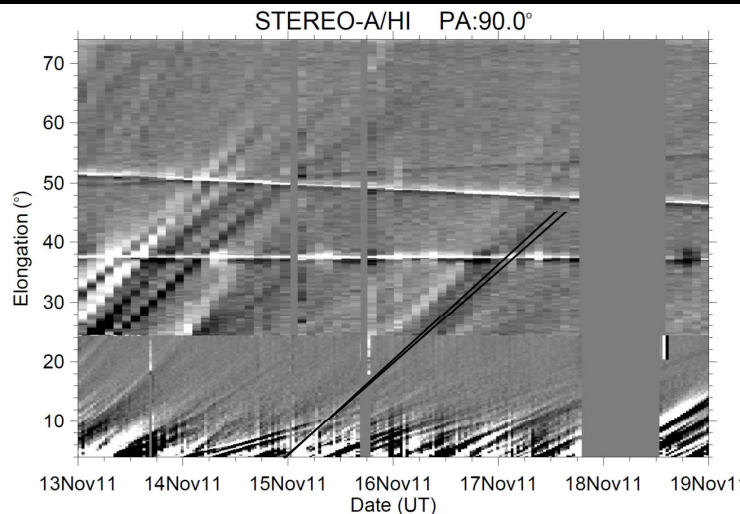
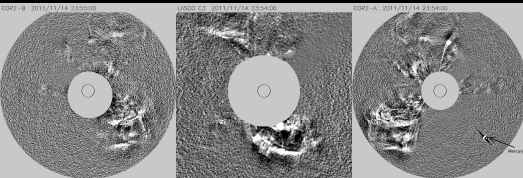
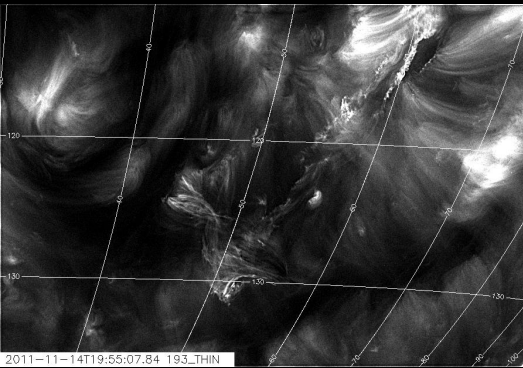
**Some Recent IPS Results and
LOFAR Technical Advances.**

IPS with LOFAR: The First CME Detection

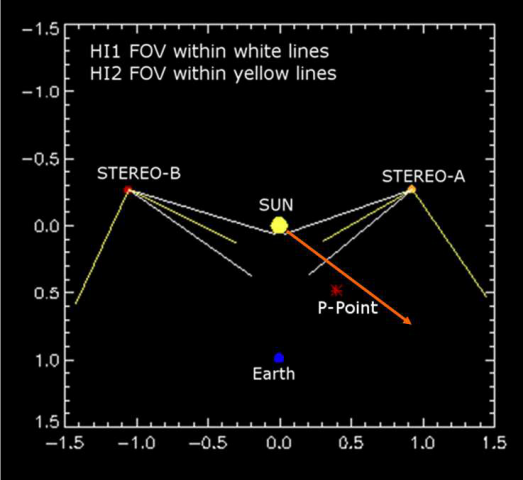
- R.A. Fallows, A. Asgekar, M.M. Bisi, A.R. Breen, S. ter-Veen, and on behalf of the LOFAR Collaboration, “The Dynamic Spectrum of Interplanetary Scintillation: First Solar Wind Observations on LOFAR”, Solar Physics “Observations and Modelling of the Inner Heliosphere” Topical Issue (Guest Editors M.M. Bisi, R.A. Harrison, and N. Lugaz), 285 (1-2), 127-139, 2013.
- Bisi, M.M., S.A. Hardwick, R.A. Fallows, J.A. Davies, R.A. Harrison, E.A. Jensen, H. Morgan, C.-C. Wu, A. Asgekar, M. Xiong, E. Carley, G. Mann, P.T. Gallagher, A. Kerdraon, A.A. Konovalenko, A. MacKinnon, J. Magdalenic, H.O. Rucker, B. Thide, C. Vocks, *et al.*, “The First Coronal Mass Ejection Observed with the LOw Frequency ARray (LOFAR)”, Submitted to The Astrophysical Journal Supplementary Series, June/July 2013 (and references therein).

The First CME with LOFAR...

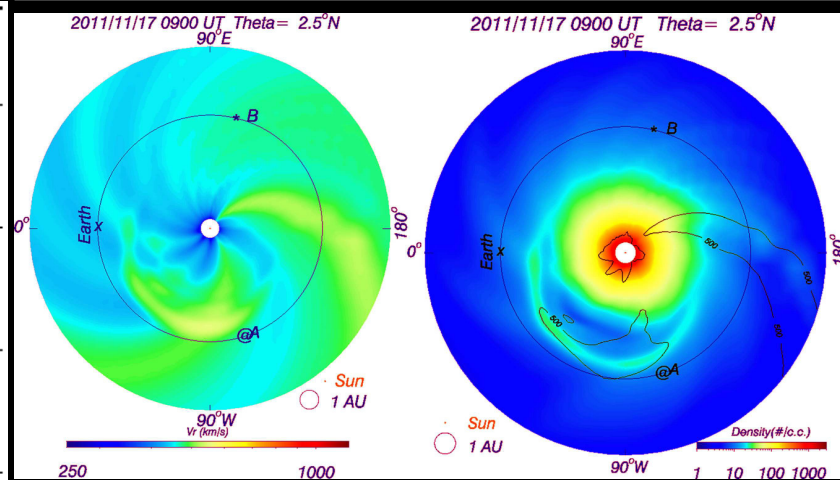
- Observations of J1256-057 (3C279) detecting a CME with LOFAR on 17 November 2011 and (briefly) its comparison so far with other remote-sensing observations and modelling.



Fully-consistent Results!

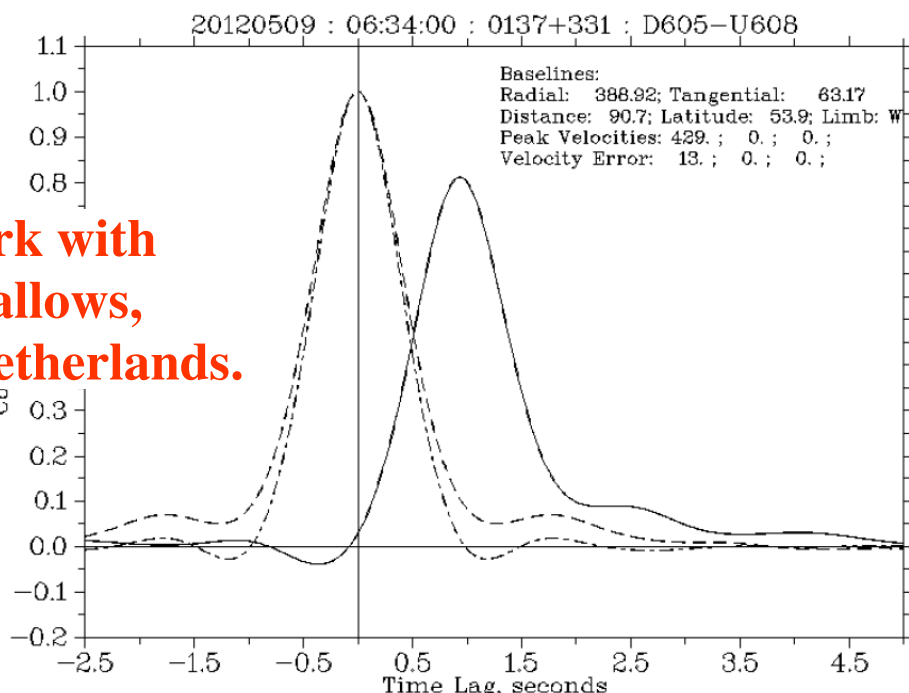
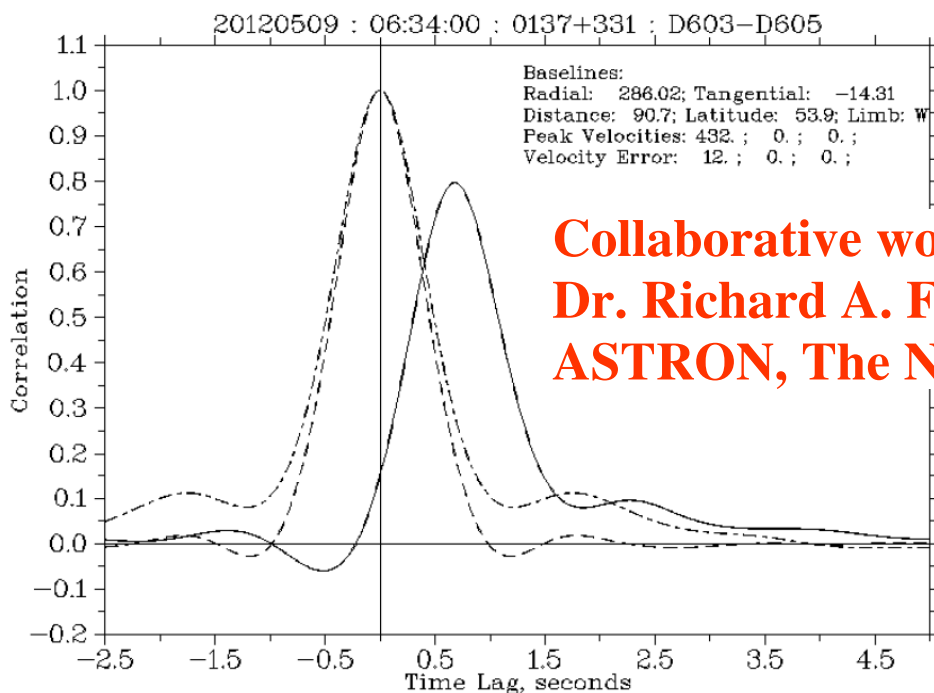


Model Used:	Best Fit in Radial Velocity (km s ⁻¹):	Error in Radial Velocity (km s ⁻¹):
<i>Front:</i>		
Fixed Phi	342.22	12.00
SSEF (30°)	348.83	12.00
Harmonic Mean	352.35	11.00
<i>Middle:</i>		
Fixed Phi	338.36	10.00
SSEF (30°)	343.61	10.00
Harmonic Mean	346.11	9.00
<i>Rear:</i>		
Fixed Phi	335.83	9.00
SSEF (30°)	343.53	8.00
Harmonic Mean	348.37	8.00

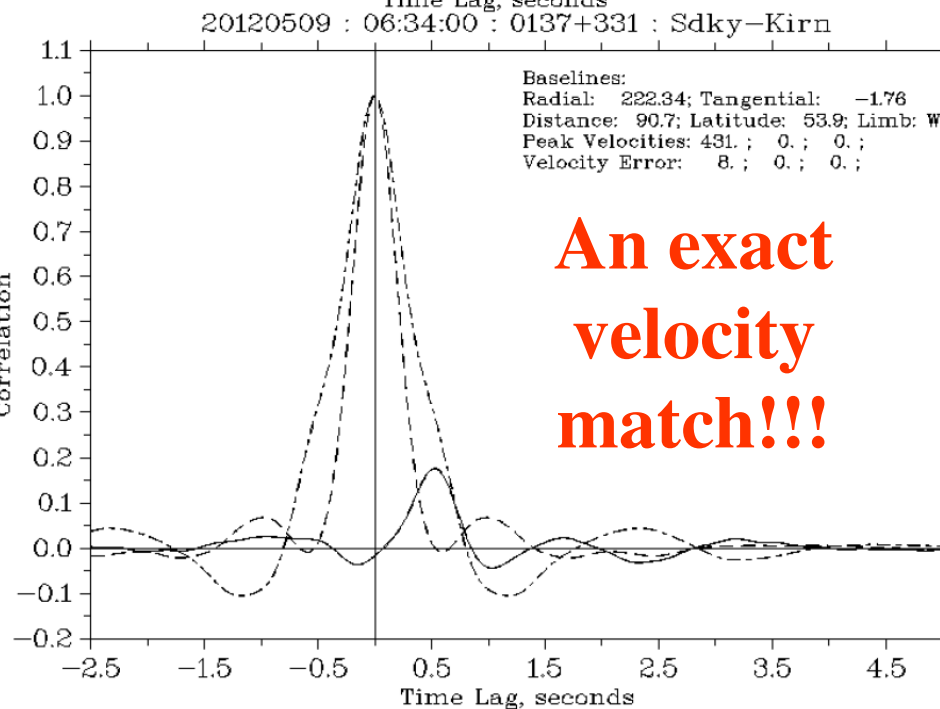
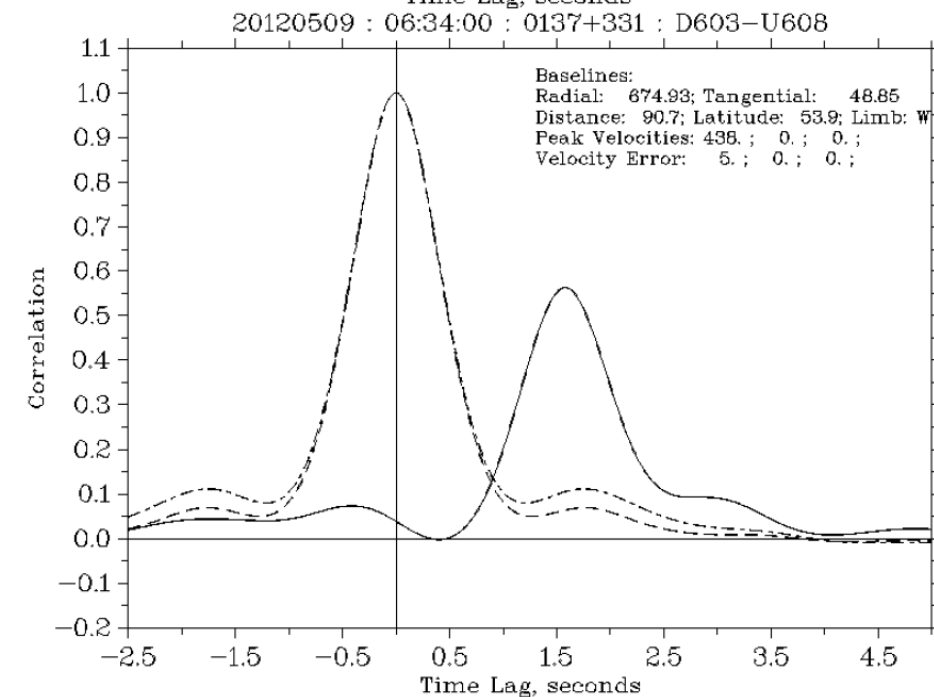


And more...

Preliminary LOFAR and EISCAT IPS Comparison



**Collaborative work with
Dr. Richard A. Fallows,
ASTRON, The Netherlands.**

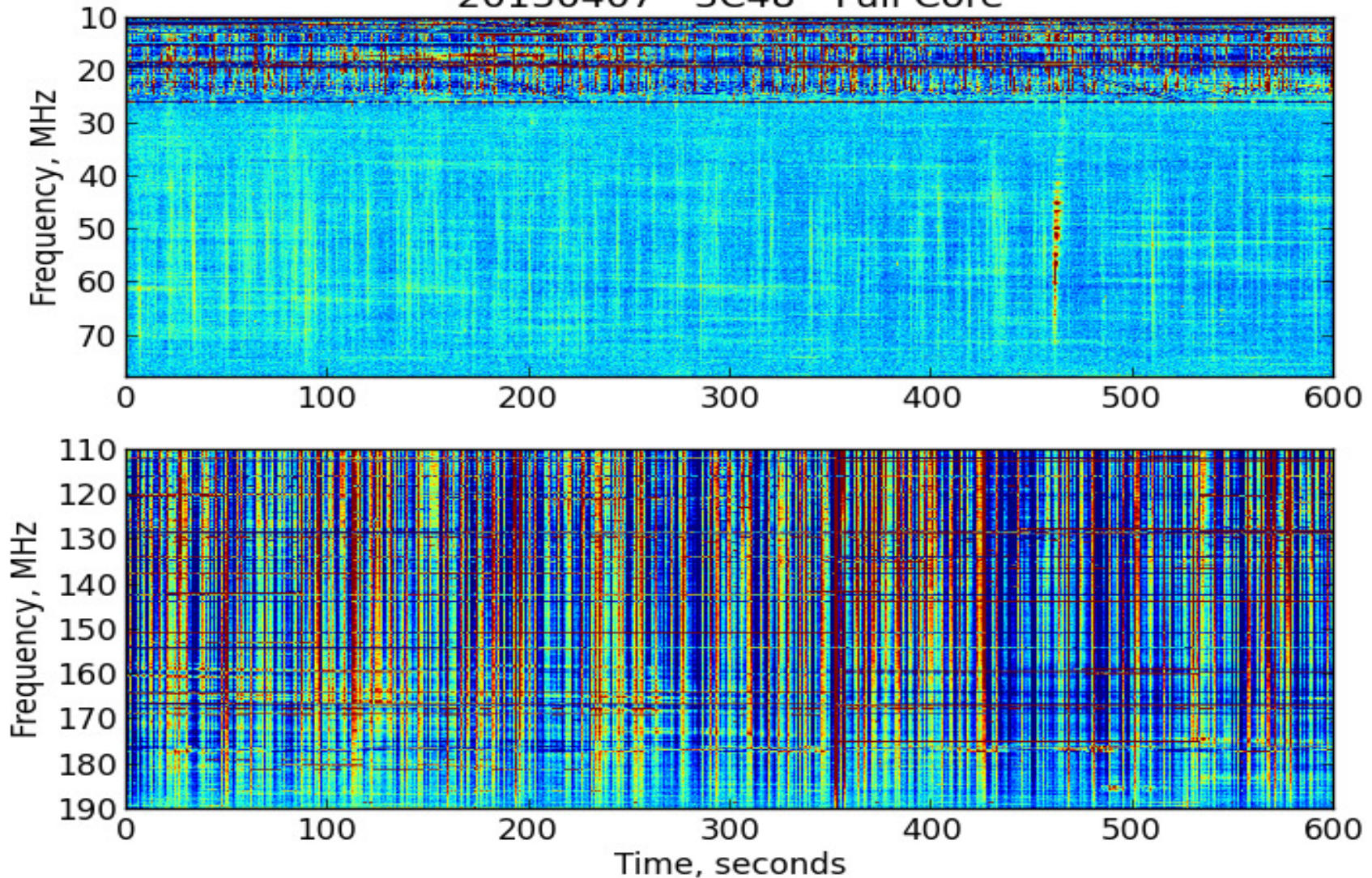


**An exact
velocity
match!!!**

LOFAR Full Core IPS Dynamic Spectrum

Courtesy of Dr. Richard A. Fallows, ASTRON.

20130407 - 3C48 - Full Core

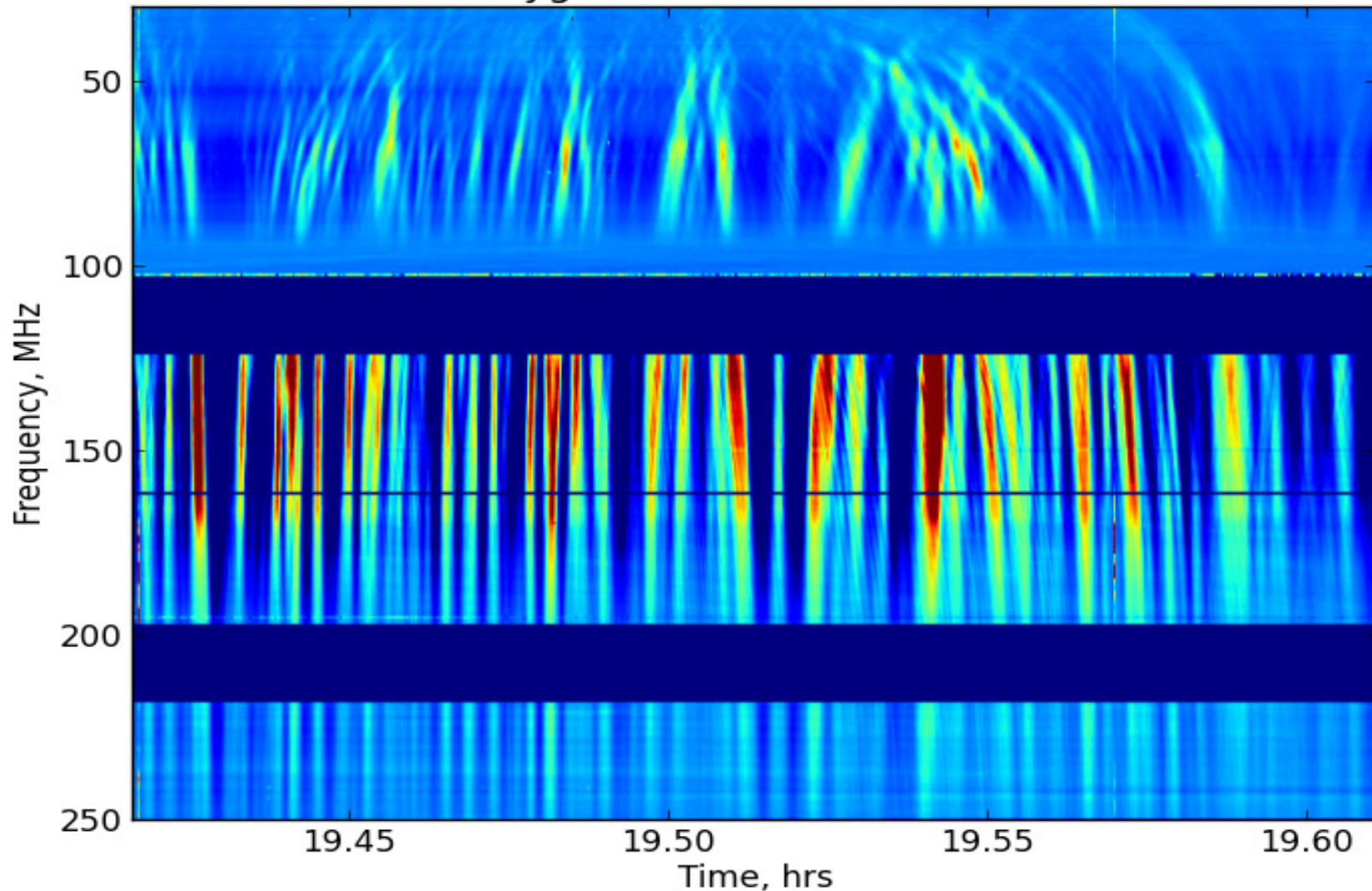


- ❖ Two separate successive observations of IPS with radio source 3C48; strong scatter seen at progressively-lower frequencies.

KAIRA Ionospheric Scintillation

More on ionospheric scintillation in the next Lecture by Norbert Jakowski.

Cyg A - 20120925 - KAIRA



- ❖ At low frequencies, the refractive effects starting to dominate at times. Courtesy of Derek MacKay/Richard Fallows, and KAIRA.

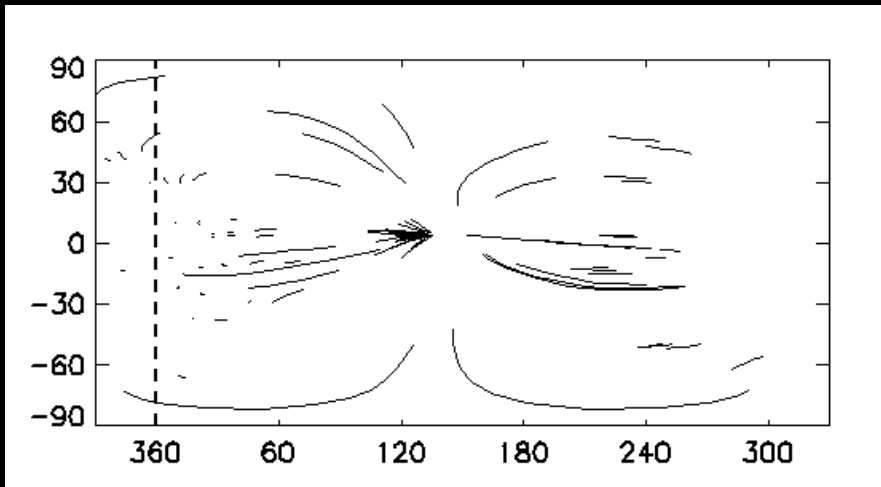
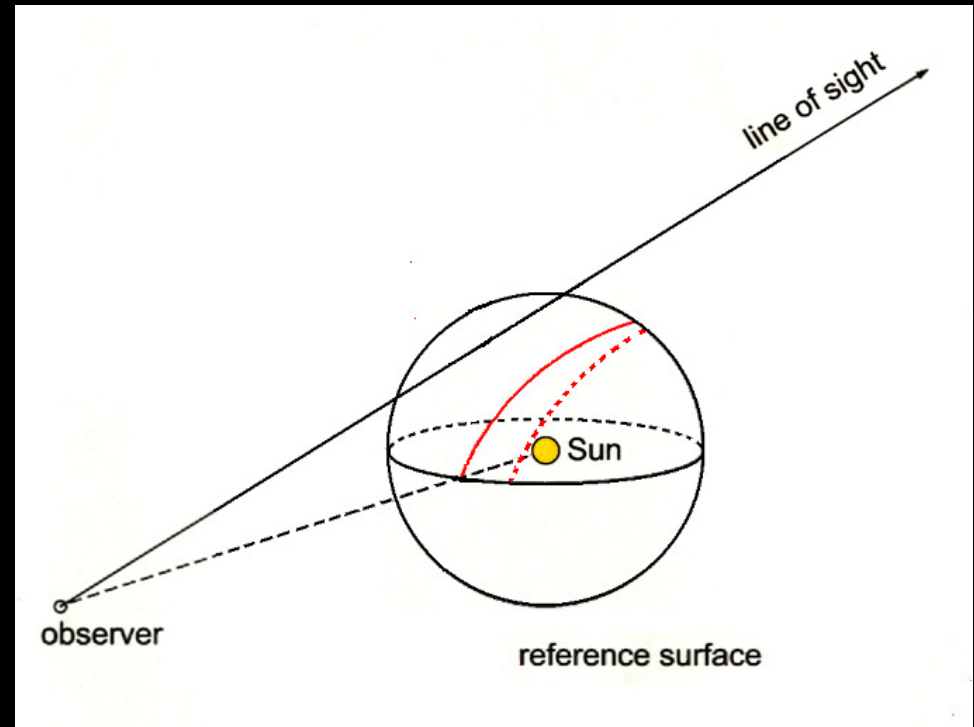
A Brief Introduction to IPS Three-Dimensional (3-D) Tomographic Reconstructions and Examples of their Usage.

This 3-D tomographic technique was developed by Dr. Bernard V. Jackson *et al.*, at the University of California, San Diego (UCSD), and is also available at NASA's CCMC. For further details see Jackson *et al.*, "Inclusion of Real-Time in-situ Measurements into the UCSD Time-Dependent Tomography and Its Use as a Forecast Algorithm", *Solar Physics*, 285 (1-2), pp.151-165, doi:10.1007/s11207-012-0102-x, 2013, and references therein.

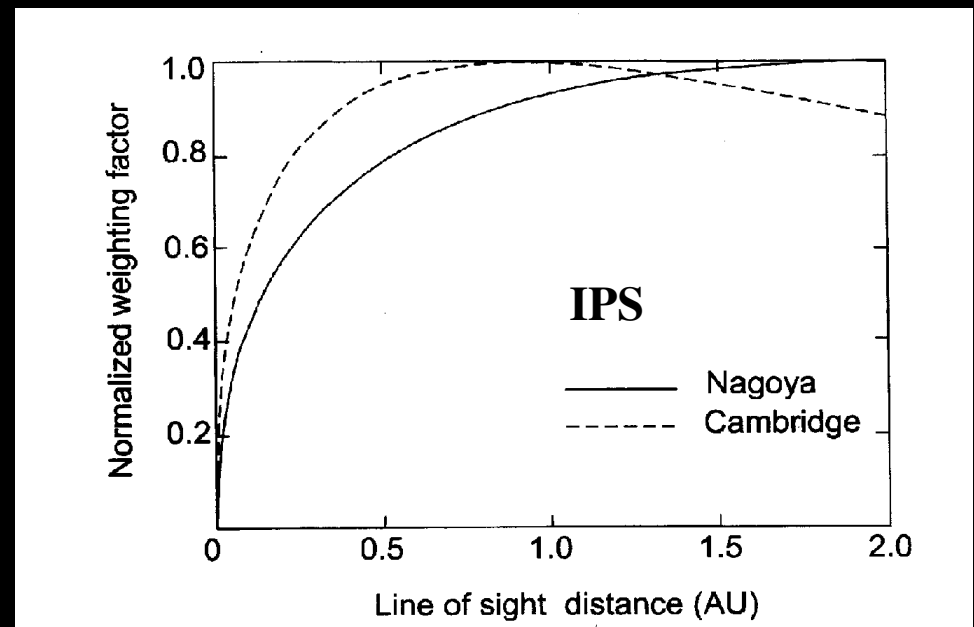
3-D Reconstructions (1)

Heliospheric Computer Assisted Tomography (C.A.T.) analyses: line-of-sight weighting values for each sky location.

STELab IPS.



14 July 2000: 00:00h-23:59h.



3-D Reconstructions (2)

- ❖ Transients (CMEs and smaller-scale features) as well as stream and co-rotating interaction region (SIR/CIR) structures can be reconstructed in terms of density and velocity using an iterative process of fitting a solar wind kinematic model (conserving mass and mass flux) to the IPS data.
- ❖ The resolution of the 3-D reconstructions will be dependent on the number of lines of sight available, *i.e.* the number of IPS data points on the sky and their even distribution.
- ❖ Whole heliosphere reconstructions (out to around 3 AU from the Sun) are possible with near-all-sky coverage.
- ❖ These reconstructions have the ability to run in a forecast mode to enable space-weather forecasting.

Periods Looked at Here...

- ❖ 2004/11/04-2004/11/08 SOlar and Heliospheric Observatory – Large Angle and Spectrometric COronagraph (SOHO/LASCO) Halo and West-limb CME events leading to large geomagnetic storms at Earth (just following the peak of solar maximum) – Ooty IPS data.
- ❖ 2008/06/02-2008/06/08 SOHO/LASCO CME (around the declining phase to solar minimum) – STELab IPS data.
- ❖ 2007/04/20-2007/05/20 Co-rotating solar-wind velocities (around the declining phase to solar minimum) – EISCAT IPS data

2004/11/04-2004/11/08 Solar and Heliospheric Observatory – Large Angle and Spectrometric COronagraph (SOHO/LASCO) Halo and West-limb CME events leading to large geomagnetic storms at Earth (just following the peak of solar maximum) – Ooty IPS data

- Bisi, M.M., R.A. Fallows, P.K. Manoharan, G.D. Dorrian, B.V. Jackson, J.M. Clover, P.P. Hick, A. Buffington, and A.R. Breen, “Solar Wind and CME Studies of the Inner Heliosphere Using IPS Data from ORT and EISCAT”, Proc. 5th Asia-Oceania Geophysical Society General Assembly, Advances in Geosciences, Volume 21: Solar & Terrestrial Science (2008), Chapter 3, pp.33-49, 2010.

- Bisi, M.M., B.V. Jackson, J.M. Clover, P.K. Manoharan, M. Tokumaru, P.P. Hick, and A. Buffington, “3-D reconstructions of the early-November 2004 CDAW geomagnetic storms: analysis of Ooty IPS speed and density data”, Annales Geophysicae, 27, pp.4479-4489, 2009.

November 2004 SOHO/LASCO C2 Events

- ❖ 2004/11/04 – 09:54 UT.
- ❖ 2004/11/04 – 23:30 UT.

- ❖ 2004/11/06 – 01:32UT.
- ❖ 2004/11/06 – 02:06 UT.
- ❖ 2004/11/07 – 16:54 UT.

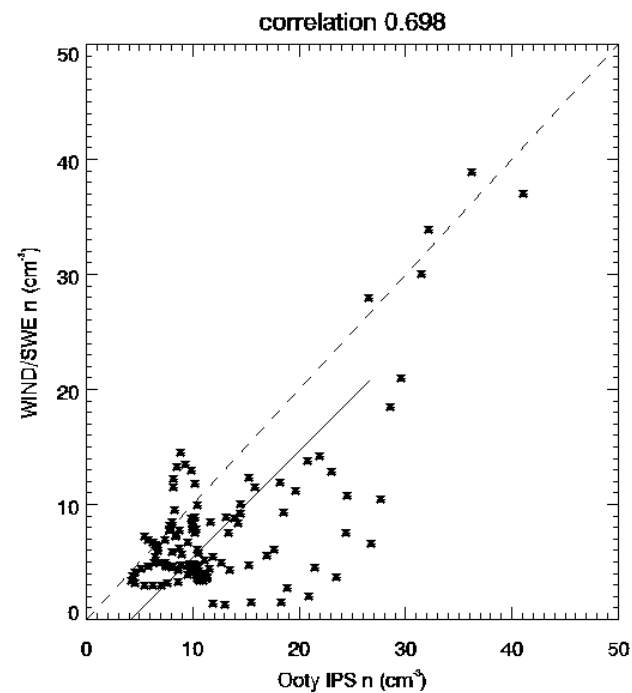
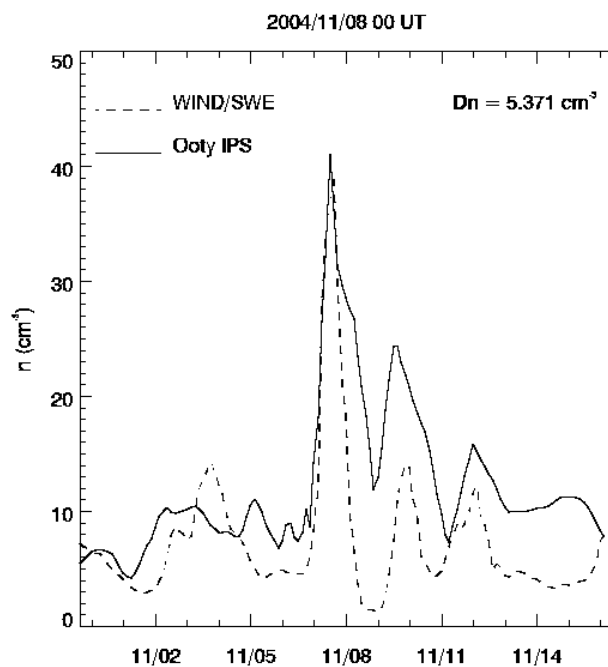
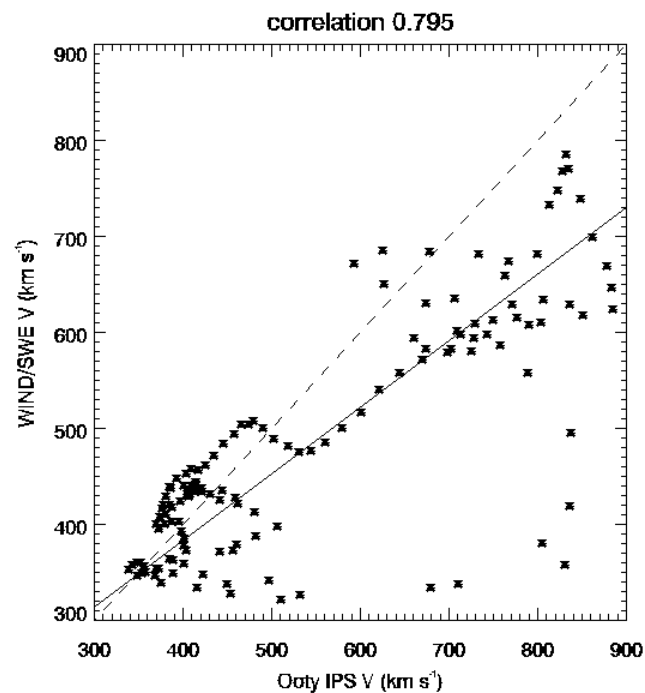
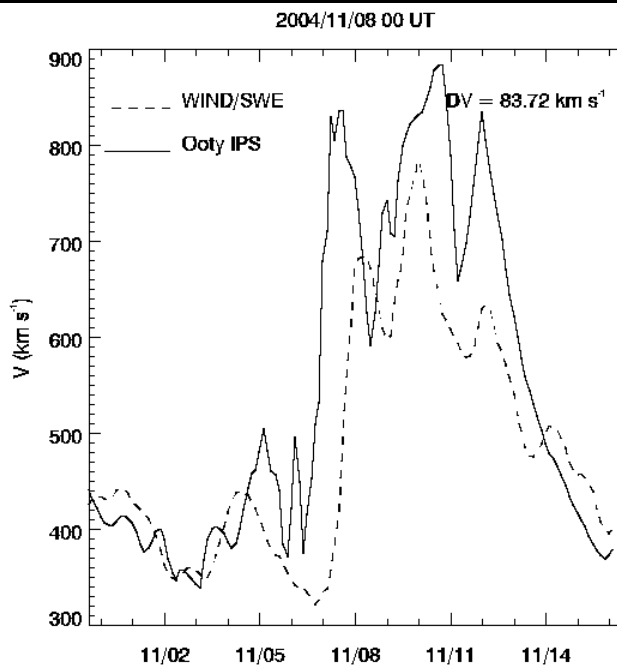
Taken from the Dr. Gareth Lawrence SOHO/LASCO CME list located at:
ftp://lasco6.nascom.nasa.gov/pub/lasco/status/LASCO_CME_List_2004.

November 2004 Earth Geomagnetic Storms

- ❖ 2004/11/08 geomagnetic storm – probably caused by the 2004/11/04 CMEs – the first Magnetic Cloud.
- ❖ 2004/11/10 geomagnetic storm – probably caused by the 2004/11/06 and 2004/11/07 CMEs – the second Magnetic Cloud.

Taken primarily from the LWS-CDAW WG1 geomagnetic storms table.

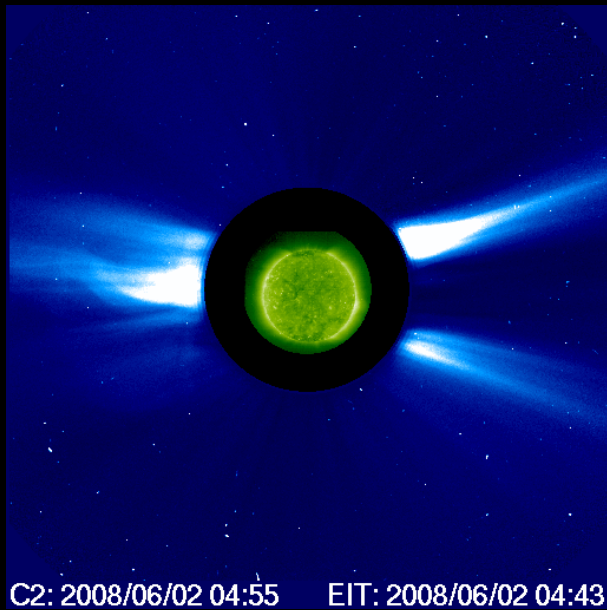
Ooty IPS 3-D Reconstructions



2008/06/02-2008/06/08 SOHO/LASCO CME (around the declining phase to solar minimum) – STELab IPS data

- Bisi, M.M., B.V. Jackson, P.P. Hick, A. Buffington, J.M. Clover, M. Tokumaru, and K. Fujiki,
“Three-Dimensional Reconstructions and Mass Determination of the 2008 June 2 LASCO
Coronal Mass Ejection using STELab Interplanetary Scintillation Observations”,
The Astrophysical Journal Letters, 715, pp.L104-L108,
doi:10.1088/2041-8205/715/2/L104, 2010.

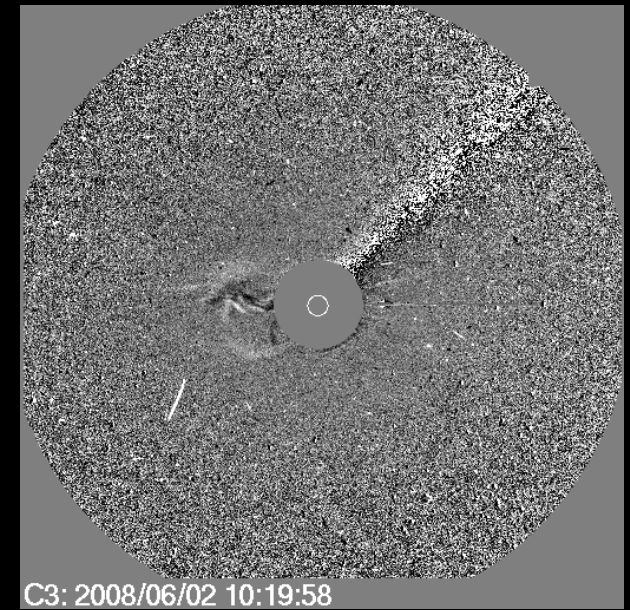
SOHO|EIT and SOHO|LASCO Images



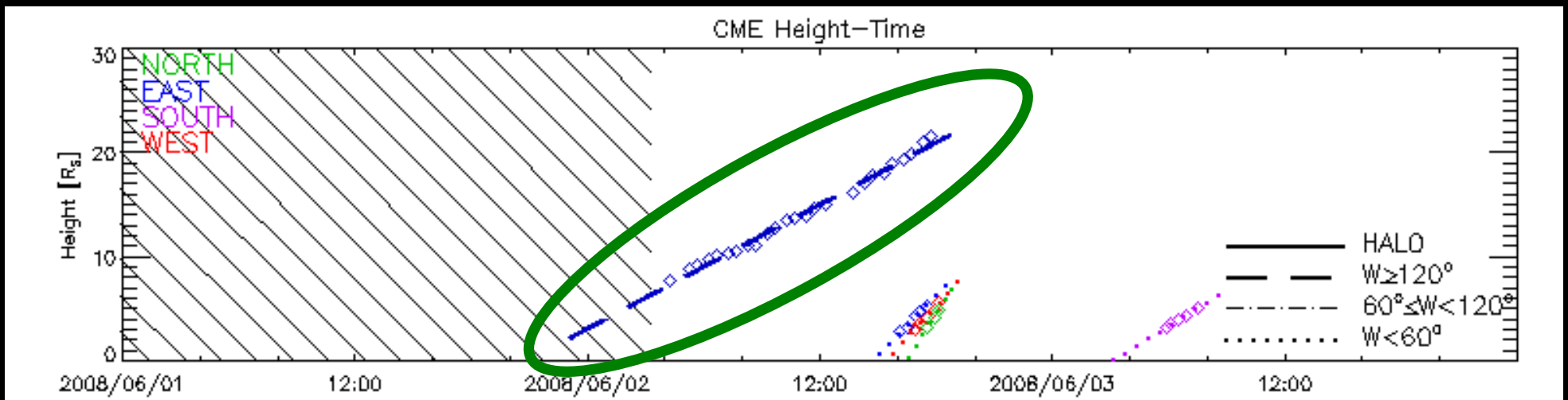
SOHO|EIT/LASCO C2
Composite Images



SOHO|LASCO C2
Difference Image

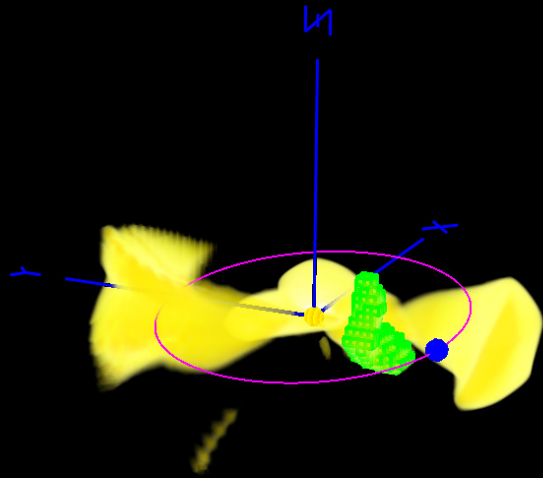


SOHO|LASCO C3
Difference Image



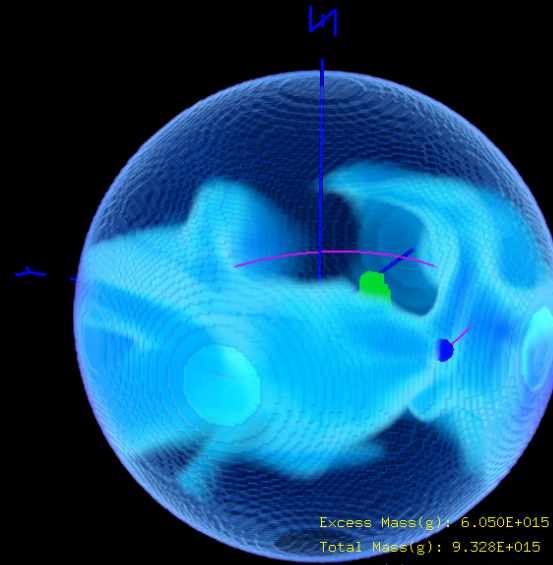
SOHO|LASCO Height-Time Plot (bottom) – All images Courtesy of CDAW CME Catalogue.

STELab IPS 3-D Reconstructions (1)



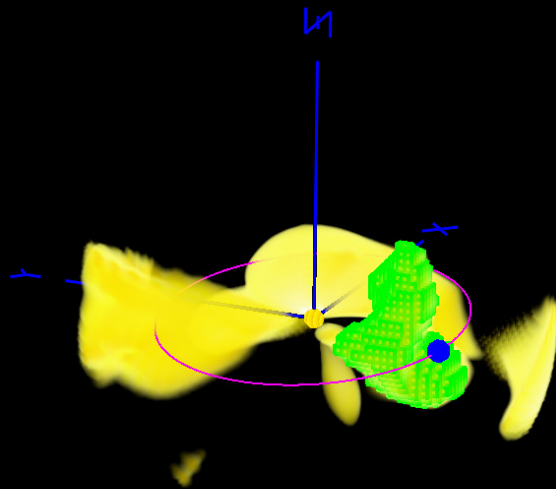
2008/06/05 03:00

Excess Mass(g): 6.050E+015
Total Mass(g): 9.328E+015
Ambient(g): 3.278E+015
energy: 4.004E+031 ergs
Volume: 0.026 AU³



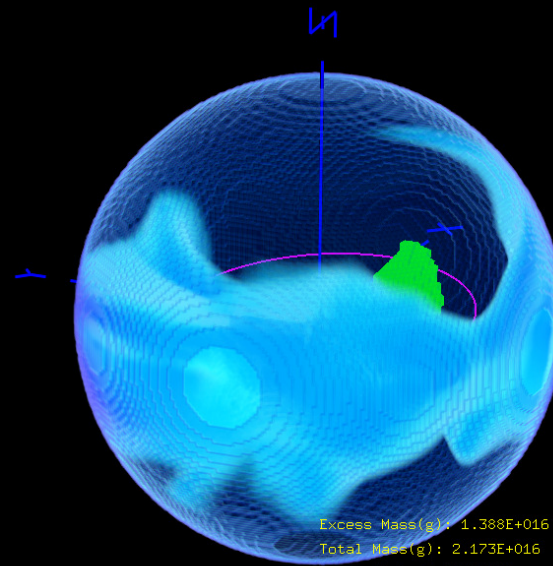
2008/06/05 03:00

Excess Mass(g): 6.050E+015
Total Mass(g): 9.328E+015
Ambient(g): 3.278E+015
energy: 2.296E+031 ergs
Volume: 0.026 AU³



2008/06/06 03:00

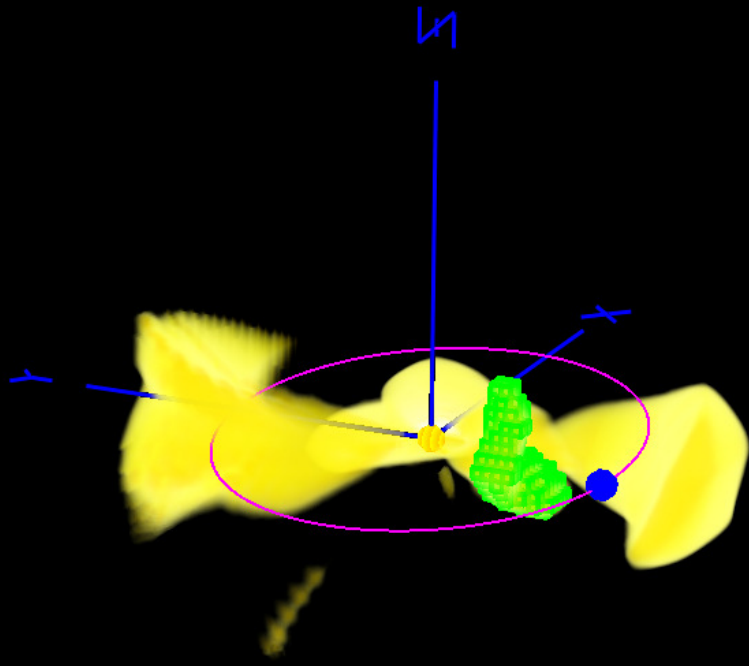
Excess Mass(g): 1.388E+016
Total Mass(g): 2.173E+016
Ambient(g): 7.843E+015
energy: 2.461E+031 ergs
Volume: 0.137 AU³



2008/06/06 03:00

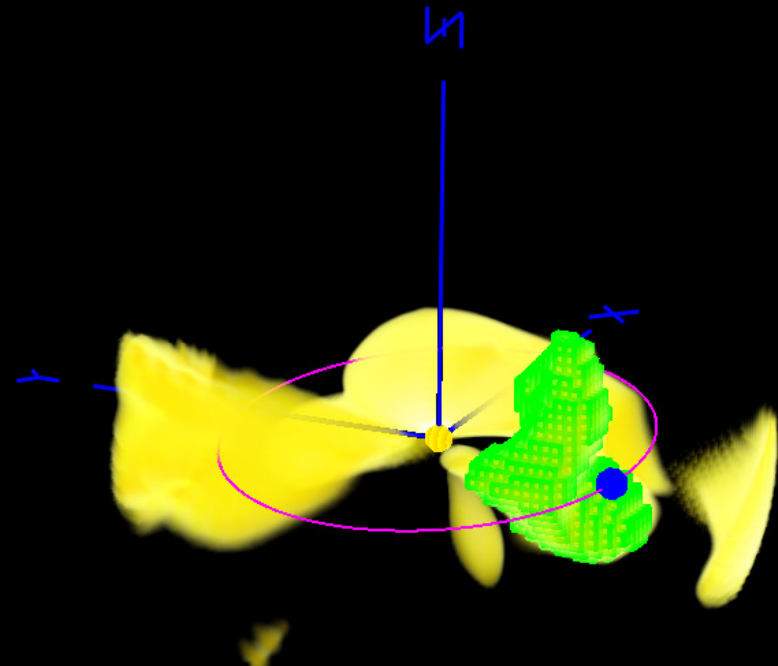
Excess Mass(g): 1.388E+016
Total Mass(g): 2.173E+016
Ambient(g): 7.843E+015
energy: 5.208E+031 ergs
Volume: 0.137 AU³

STELab IPS 3-D Reconstructions (2)



Excess Mass(g): 6.050E+015
Total Mass(g): 9.328E+015
Ambient(g): 3.278E+015
energy: 4.004E+031 ergs
Volume: 0.026 AU³

2008/06/05 03:00



Excess Mass(g): 1.388E+016
Total Mass(g): 2.173E+016
Ambient(g): 7.843E+015
energy: 2.461E+031 ergs
Volume: 0.137 AU³

2008/06/06 03:00

STELab reconstructed isolated ICME portion at around 0.7 AU (left) and 0.9 AU (right).

CME mass from CDAW CME List (LASCO) = 4.7×10^{14} g (CDAW);

CME mass from STEREO COR-1A = 7.5×10^{14} g (Robbrecht *et al.*, 2009);

CME mass from STEREO COR-2A = 3.5×10^{15} g (Robbrecht *et al.*, 2009);

ICME mass from STELab 3-D reconstruction near 0.7 AU = 6.1×10^{15} g;

ICME mass from STELab 3-D reconstruction near 0.9 AU = 1.4×10^{16} g (Bisi *et al.*, 2010);

(Excess mass above the ambient is what is being shown as the CME/ICME mass).

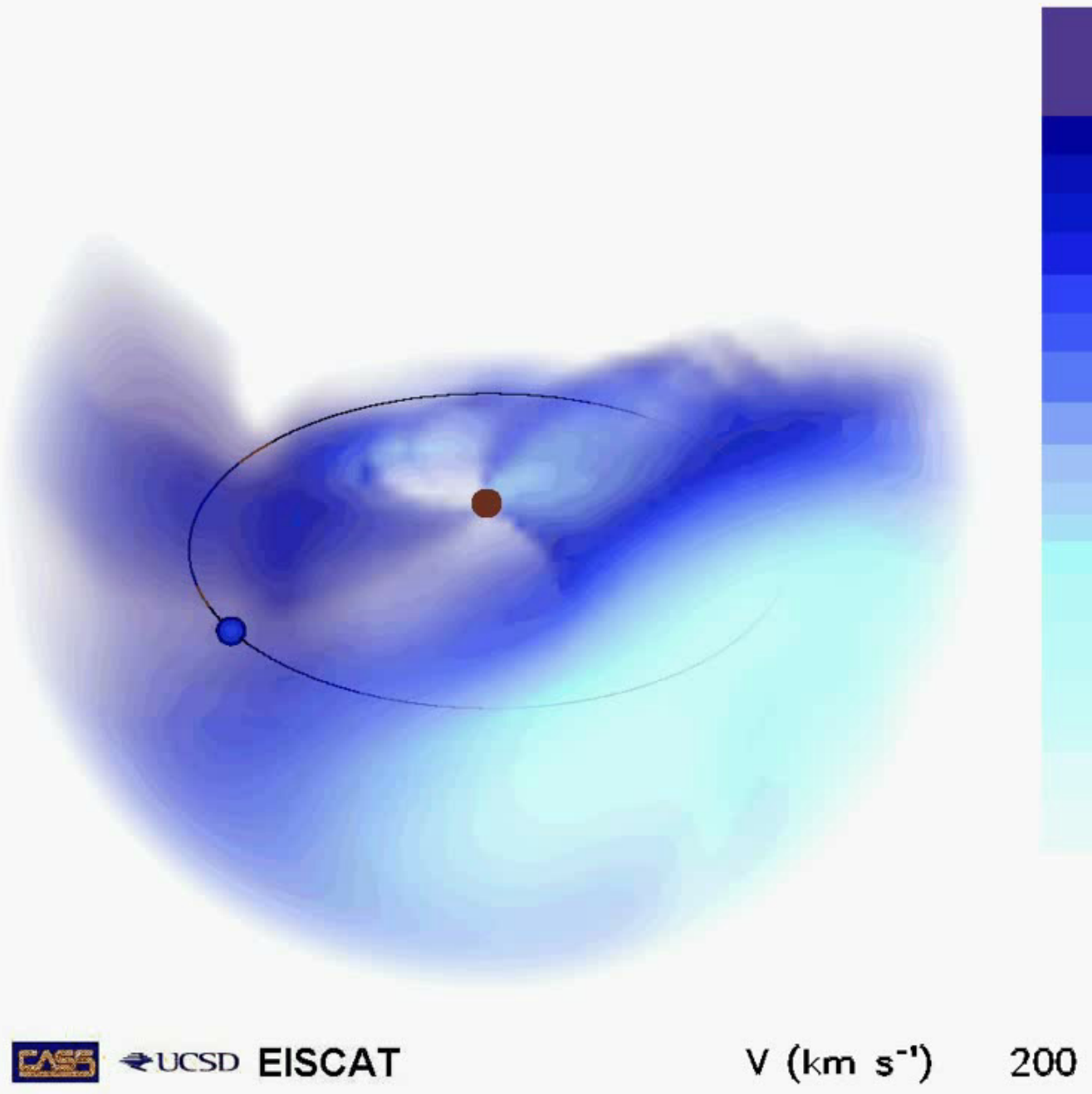
2007/04/20-2007/05/20 Co-rotating solar-wind velocities (around the declining phase to solar minimum) – EISCAT IPS data

- Bisi, M.M., B.V. Jackson, A.R. Breen, G.D. Dorrian, R.A. Fallows, J.M. Clover, and P.P. Hick, “Three-Dimensional (3-D) Reconstructions of EISCAT IPS Velocity Data in the Declining Phase of Solar Cycle 23”, Solar Physics “Remote Sensing of the Inner Heliosphere” Topical Issue (Guest Editors M.M. Bisi and A.R. Breen), 265 (1-2), pp.233-244, doi:10.1007/s11207-010-9594-4, 2010.

EISCAT IPS 3-D Velocity Reconstruction

2007/04/17 23:00

400



UCSD EISCAT

V (km s⁻¹)

200

**A Brief Introduction to Heliospheric
Faraday Rotation (FR) and Initial Progress
Towards Heliospheric FR Determination.**

(Who can tell me what Faraday rotation is?)

Heliospheric Faraday rotation (FR) (1)

- ❖ FR is the rotation that occurs as an electromagnetic (EM) wave traverses a birefringent medium such as the solar-wind plasma.
- ❖ Coronal FR from spacecraft beacons at superior conjunction (solar occultation) – solar scintillation effects at X and Ka bands.
- ❖ Attempt to determine the rotation measure (RM) of a polarised radio source to derive the heliospheric Faraday rotation (FR) caused by features, such as coronal mass ejections (CMEs), travelling out in the solar wind responsible for Space Weather at the Earth along with solar wind interaction regions.
- ❖ Implications for Space-Weather forecasting at the Earth.
- ❖ FR along a LOS is the integrated product of the electron density (determined using IPS through 3-D tomographic reconstruction, or from white-light imagery) and the component of the solar magnetic field parallel to the wave vector of the EM wave.

Heliospheric FR (2)

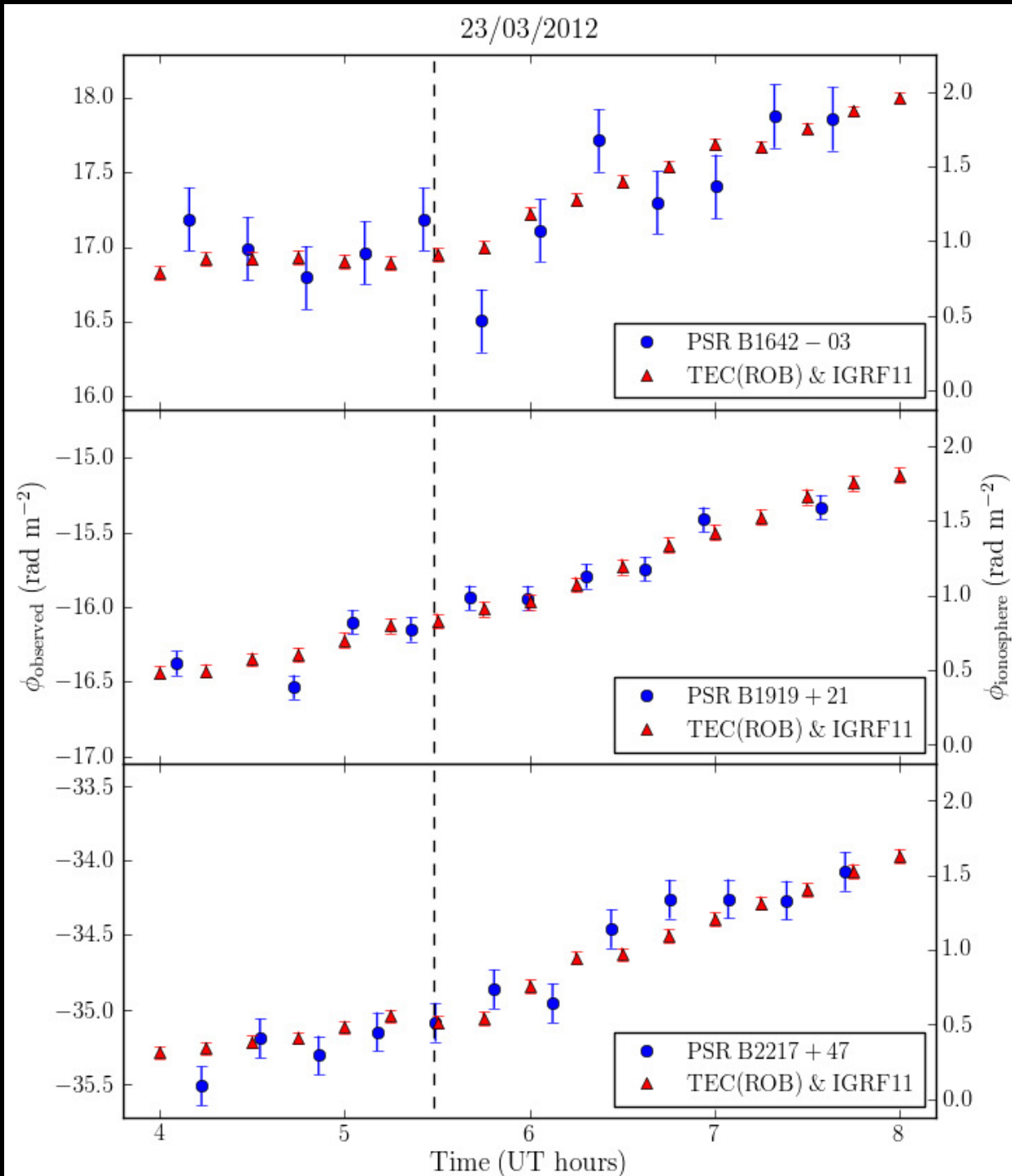
- ❖ As a polarised EM wave from radio source propagates through the birefringent plasmas of the heliosphere and Earth's ionosphere, the plane of polarisation of the EM wave rotates as a function of the magnetic field “frozen-in” to the plasma.
- ❖ Dominant FR signatures during geomagnetic activity will likely arise from Earth's ionosphere plus constant FR of the source due to the Interstellar Medium (ISM); the heliospheric contributions for LOFAR/MWA frequencies could be small by comparison.
- ❖ When a CME, propagating outward from the Sun (in an assumed radial outflow), crosses the observing LOS to the radio source over a period of time, the FR changes due to fluctuations in the electron density and the component of the magnetic field within the CME (or solar wind) structure flowing across the LOS – this is the heliospheric FR component that we're after...

Calibrating FR by Understanding the Ionospheric Contribution for the RM of Polarised Pulsar Observations

- Sotomayor-Beltran, C., C. Sobey, J.W.T. Hessels, G. de Bruyn, A. Noutsos, *et al.*, “Calibrating high-precision Faraday rotation measurements for LOFAR and the next generation of low-frequency radio telescopes”, *Astronomy & Astrophysics*, 552, A58, 1-13, 2013.

Heliospheric FR Progress (1)

Observed Faraday depths, ϕ_{observed} , each using 12 observations with LOFAR Superterp HBA (top and bottom) and LBA (middle) with the ionFR-modelled ionospheric Faraday depths, $\phi_{\text{ionosphere}}$, toward three pulsars (as labelled) as a function of time during sunrise (marked by the vertical dashed line).
Observations: blue circles – left-hand axis labels; and model: red triangles – right-hand axis labels).

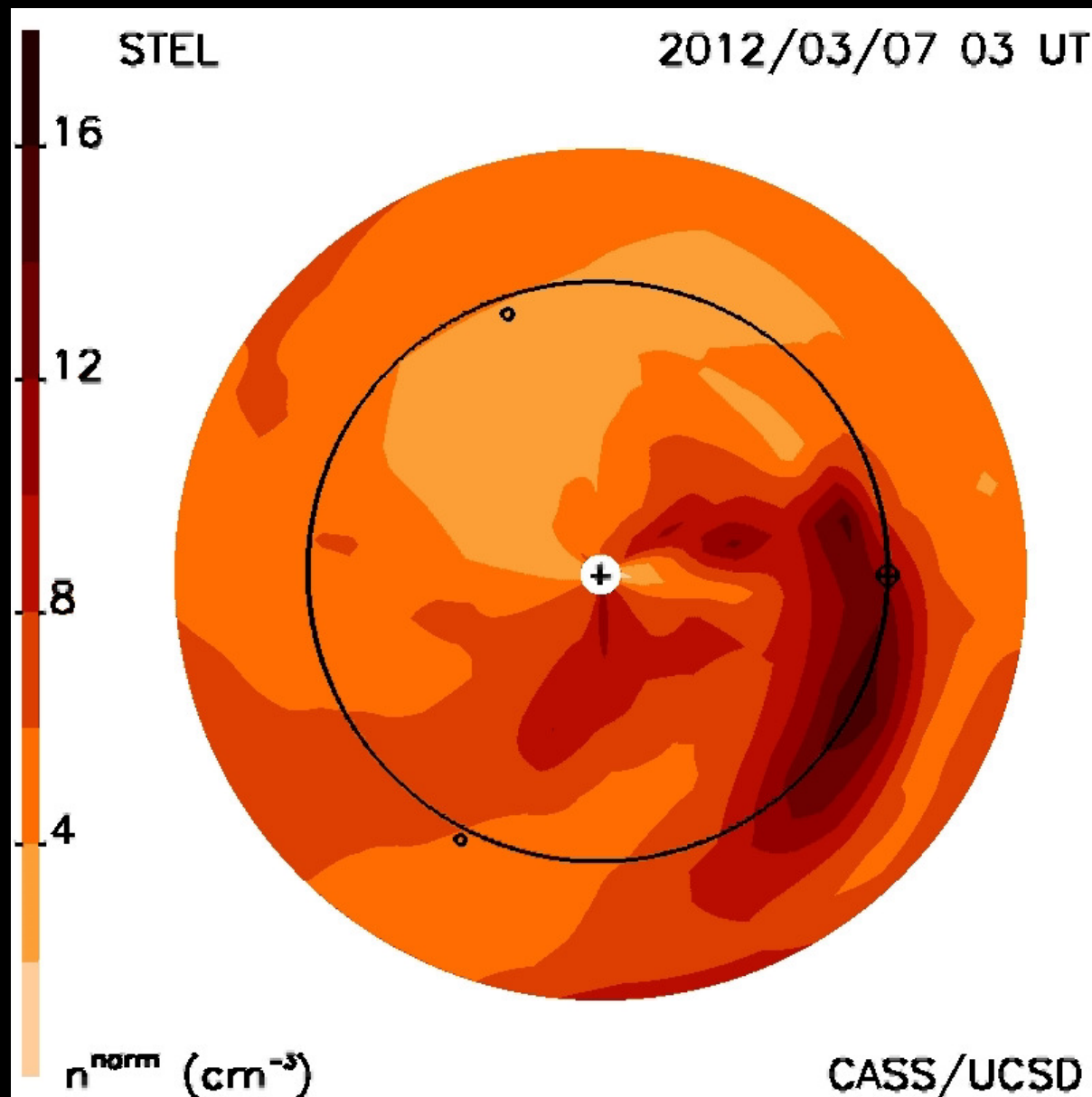


Heliospheric FR Progress (2)

- ❖ For the case of a single polarised source positioned behind one or more ionised plasmas that are not emitting polarised radiation, the Faraday depth of the source is equivalent to its RM.
- ❖ The modelled ionosphere RM in each case shown here is approximately the same for each observation (as expected) with it resulting in $\sim 5\%$ to $\sim 15\%$ of the RM due to the IsM.
- ❖ If you remove the ionospheric RM from the total RM then you are left with a near-flat and constant RM with perhaps a very small rise into the day side of observations.
- ❖ Heliospheric RM contribution is likely to be a fraction of the ionospheric contribution and so will likely only be seen as a deviation from the generally-flat RM response to the IsM if the ionospheric contributions are correctly removed.

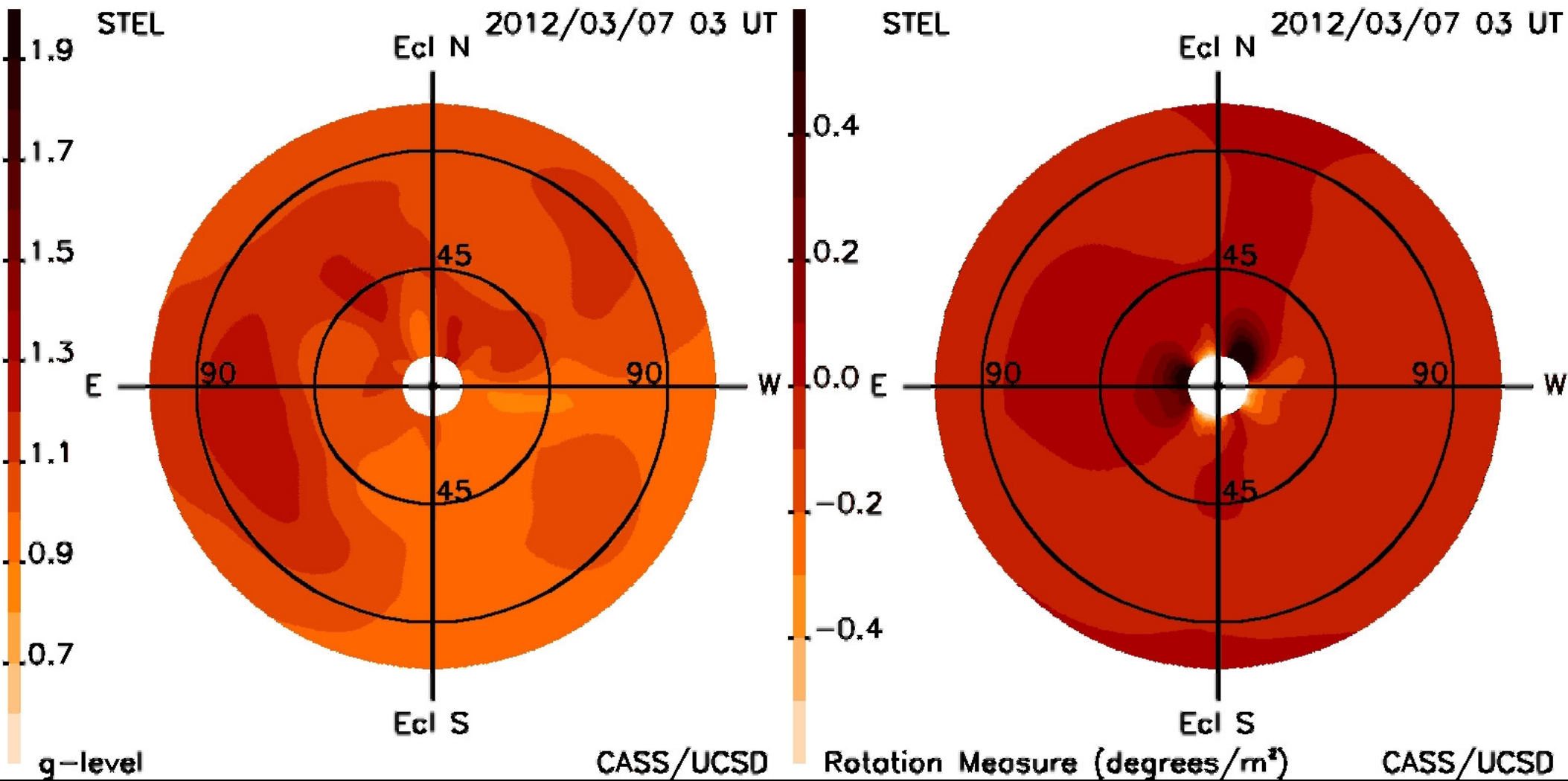
And more...

More IPS UCSD 3-D Tomography (1)



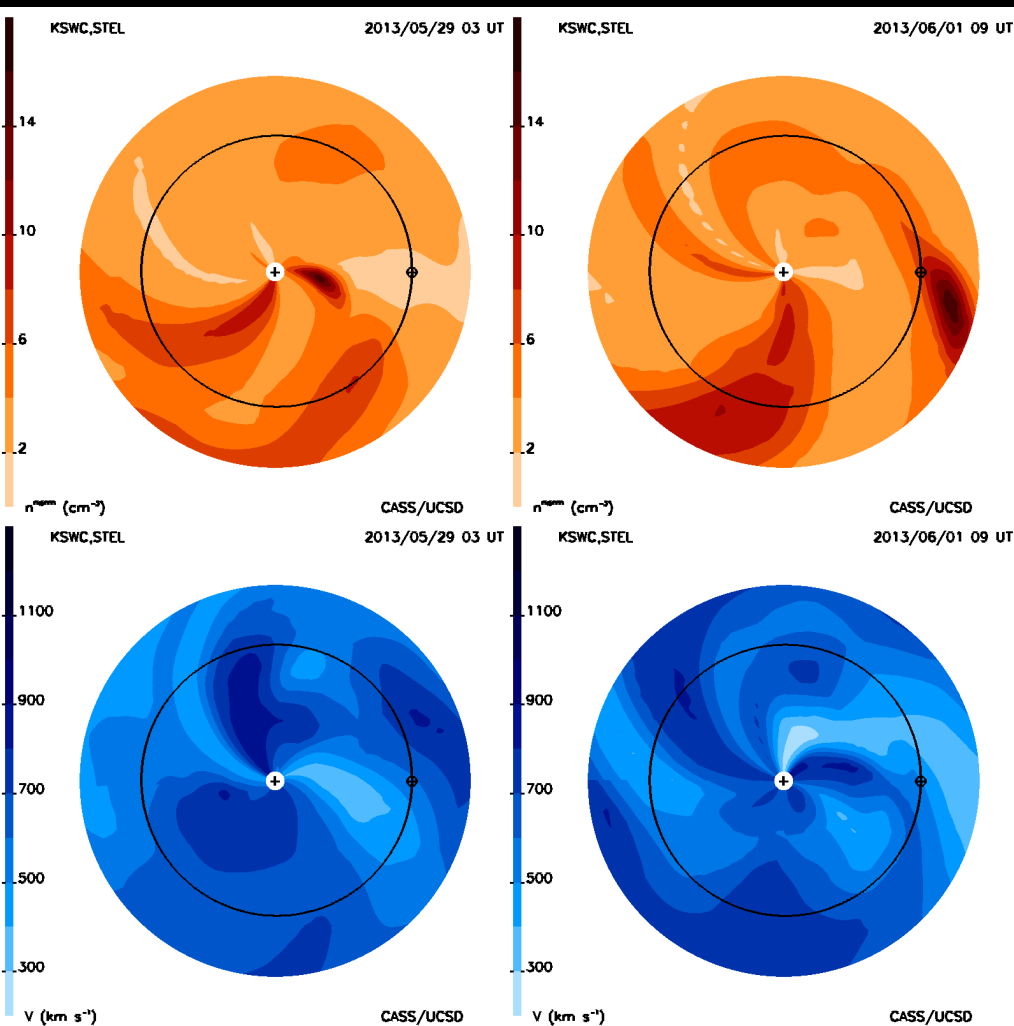
- ❖ 3-D reconstructions of Carrington rotation (CR) 2121 showing a CME of interest from 07 March 2012 launched around 01:00UT.

More IPS UCSD 3-D Tomography (2)



- ❖ The same period extracted from CR2121 comparing IPS g-level fisheye sky map (left) with that of reconstructed RM from ambient magnetic fields (right) perturbed by the CME.

More IPS UCSD 3-D Tomography (3)



❖ This strange geostorm-causing event where the driver was missed by most – forecasters, modellers, and observers alike (but not real-time UCSD tomography) – likely a combination of CME and CIR.

KORCAI

Space

Weather

Center

(KSWC

): An

implem

entation

of the

UCSD

IPS

Tomogr

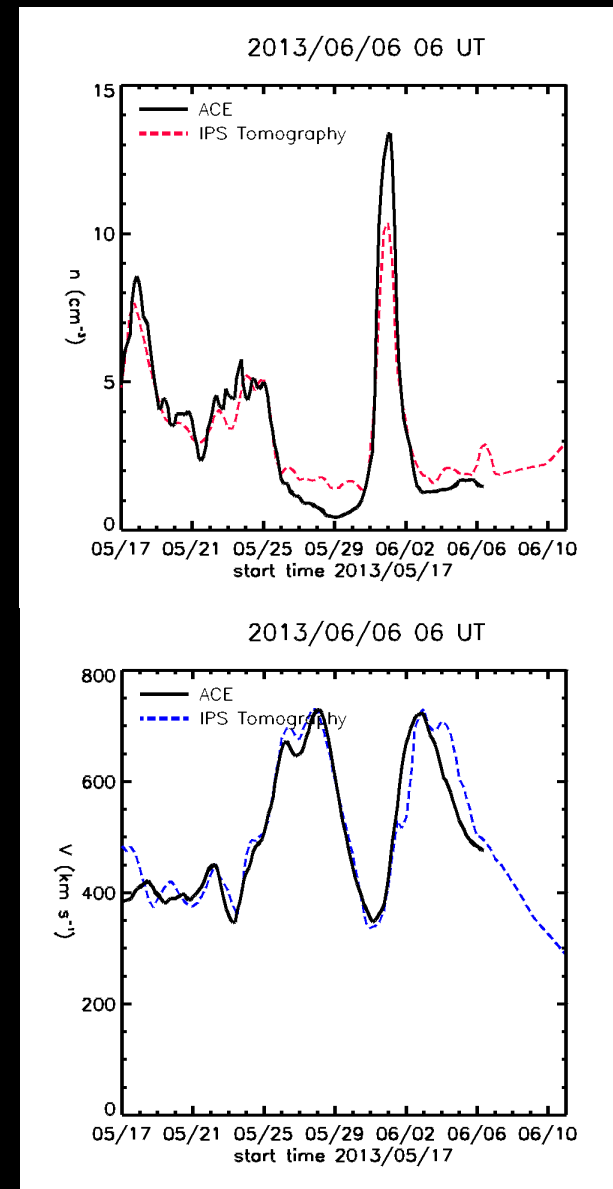
aphy

incorpo

rating

ACE

real-time



Lecture Summary.

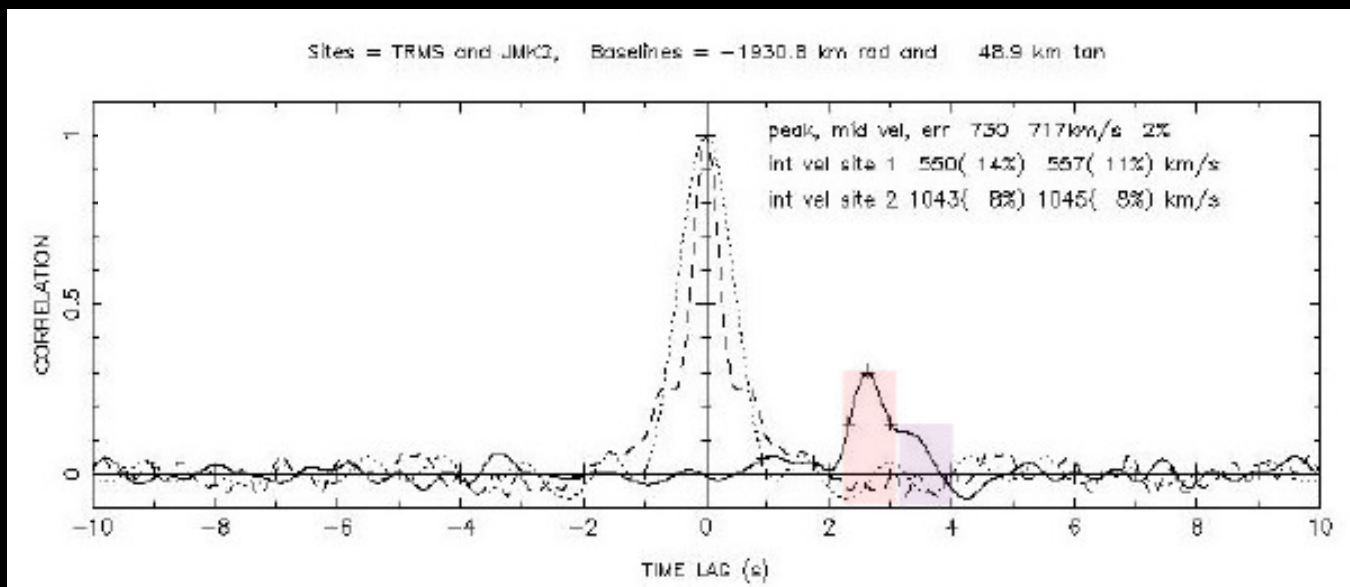
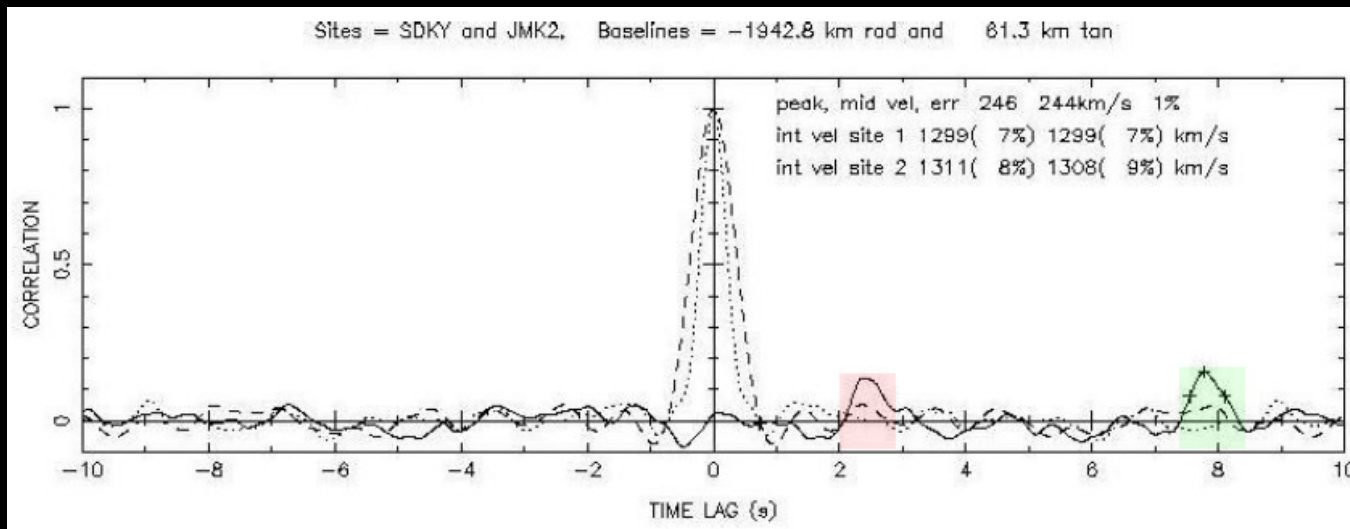
Bisi Lecture Summary (1)

- ❖ Both planetary and solar occultation experiments provide us an ability to measure and learn about the respective ionospheres and atmospheres, or both (in the case of planets where both exist).
- ❖ IPS is an extremely-powerful and unique technique for making remote-sensing observations of the inner heliosphere.
- ❖ IPS on LOFAR is progressing very well with good early solar wind and CME results, including an exact comparison with well-known EISCAT observations of IPS over multiple frequencies.
- ❖ Planning underway for LOFAR observations of Heliospheric FR.
- ❖ UCSD tomography will provide an excellent way of obtaining magnetic-field values from combined observations of FR and IPS.

Bisi Lecture Summary (2)

- ❖ The basics of the theory behind IPS are covered in the slides. Observations of IPS allow us to probe the heliosphere over a wide range of distances from the Sun at almost all latitudes (depending on the observing frequency and astronomical source locations on the sky).
- ❖ There are various forms of scintillation that occur in radio waves throughout the Heliophysics system and beyond (solar, interplanetary, planetary, ionospheric, stellar, and interstellar).
- ❖ A combination of IPS and heliospheric FR incorporating the use of white-light imager information, could provide a pathway to the remote-sensing and prediction of incoming magnetic-field (namely B_z) with large implications and potential advances for space-weather forecasting!

And Some Not-So-Random Images...



Thanks for Listening!!!

URLs: <http://www.spacephysicist.com/>
and <http://ips.ucsd.edu/>.

*Some example cross-correlation functions from
EISCAT-MERLIN multi-site extremely-long
baseline (ELB) IPS analyses.*